



Cite this: DOI: 10.1039/d3ee01325a

# Design and synthesis of triboelectric polymers for high performance triboelectric nanogenerators

Xinglin Tao,<sup>ab</sup> Xiangyu Chen <sup>\*ab</sup> and Zhong Lin Wang <sup>\*abc</sup>

Triboelectric polymer materials are an essential element for triboelectric nanogenerators (TEGs). The design and synthesis strategies of triboelectric polymers are the foundation for improving the performance of TEGs and the related fabrication methods are also a key element for scaling up the industrial applications of TEGs. Moreover, the mechanism of charge accumulation, dissipation, and migration occurring during the contact electrification of triboelectric polymers can also inspire other studies of polymer electronic devices. Herein, a review focusing on the latest progress in the triboelectric polymers towards high performance TEG devices is presented. The development and the application of highly negatively/positively charged polymers, covalent organic frameworks (COFs), adjustable copolymers, and robust composite materials are systematically discussed. The important experimental strategies and conclusions of triboelectric polymers are also summarized to guide future studies. This review can be helpful for the research on diversified TEGs and also facilitate studies in many fields related to the polymer materials. Finally, the challenges and prospects of the development of triboelectric polymers for high performance TEGs are outlined, including the influence factor of chemical structure on electrification polarity, elevation of charge density and charge stability, and large-scale and low-cost synthesis approaches.

Received 27th April 2023,  
Accepted 21st June 2023

DOI: 10.1039/d3ee01325a

rsc.li/ees

## Broader context

The triboelectric materials are the very foundation of the triboelectric nanogenerator (TENG) technique, which determine not only the output performance but also the diversified functions of TENG devices. Polymers are the major materials for fabricating TENGs owing to their advantages of high charge density, flexibility, cost-effectiveness, and light weight. The design and synthesis strategies of triboelectric polymers are the foundation for improving the performance of TENGs and the related fabrication methods are also the key element for scaling up the industrial applications of TENGs. Moreover, the research on the triboelectric property of polymers can also elucidate the understanding about the interfacial charge accumulation, migration, and dissipation of polymer materials, which may also supplement the study of polymers' electrical properties. The mechanism of charge accumulation, dissipation, and migration occurring during the contact electrification of triboelectric polymers also requires a systematic discussion and summary to facilitate subsequent research.

## 1. Introduction

Triboelectric nanogenerators (TEGs), which were first invented in 2012,<sup>1,2</sup> are a promising technology to harvest mechanical energy from surroundings or biological motion and convert it into electricity.<sup>3–5</sup> Owing to the advantages of remarkable conversion efficiency for low-frequency vibrations,

high voltage, low cost, and a wide selection of triboelectric materials, TENGs have developed rapidly and become a promising technology to apply in micro–nano energy harvesting,<sup>6,7</sup> self-powered sensing,<sup>8,9</sup> blue energy,<sup>10,11</sup> high voltage sources, *etc.*<sup>12,13</sup> Over the past decade, the development of TENGs has been strongly driven by collaborative advances in triboelectric materials,<sup>14,15</sup> mechanical structure design,<sup>16,17</sup> power management,<sup>18,19</sup> and application exploration.<sup>20</sup> The triboelectric materials are the very foundation of the TENG technique, which determine not only the output performance but also the diversified functions of TENG devices.<sup>21,22</sup> Polymers are the major materials for fabricating TENGs and the study of triboelectric polymers has attracted tremendous attention owing to their advantages of high charge density, flexibility, cost-effectiveness, and light weight.<sup>23</sup> The research on advanced

<sup>a</sup> CAS Center for Excellence in Nanoscience, Beijing Key Laboratory of Micro-nano Energy and Sensor, Beijing Institute of Nanoenergy and Nanosystems, Chinese Academy of Sciences, Beijing 100083, P. R. China.

E-mail: chenxiangyu@binn.cas.cn, zhong.wang@mse.gatech.edu

<sup>b</sup> School of Nanoscience and Engineering, University of Chinese Academy of Sciences, Beijing 100049, P. R. China

<sup>c</sup> School of Materials Science and Engineering, Georgia Institute of Technology, Atlanta, Georgia 30332-0245, USA

triboelectric polymers, especially the systematic design and synthesis methods, is the main study branch of TENGs to fulfil the real application and scale-up manufacturing of diversified TENG devices.<sup>24</sup> Moreover, the relationship between the chemical structure of polymers on the nanoscale and their electrification capability on the macroscale also needs to be summarized and further explored, in order to obtain a clear picture of the mechanism of contact electrification.

On the other hand, polymer science has expanded quickly in the past century, starting from the fundamental understanding of polymerization in the 1920s<sup>25</sup> to creating materials that almost cover all aspects in current life, including plastic, rubber, fibre, coatings, composites, and adhesives.<sup>26–28</sup> In recent years, one of the key aspects of polymer research focuses on enriching the applications of polymers in the field of energy and electronic devices, such as capacitors or batteries,<sup>29–34</sup> fuel cells,<sup>35,36</sup> organic photovoltaics,<sup>37–39</sup> organic light emitting diodes,<sup>40,41</sup> and even polymer electronic skin.<sup>42–44</sup> Then, with the emergence of the TENG technique, polymers with excellent triboelectric properties can be further exploited as a kind of functional material to be applied in the field of self-powered sensing and distributed power generation.<sup>45–52</sup> Accordingly, the research on the triboelectric property of polymers can also elucidate the understanding about interfacial charge accumulation, migration, and dissipation of polymer materials, which may also promote the study of other polymer electronic devices. Therefore, the progress in design and synthesis of triboelectric polymers not only benefits the development of high performance TENGs, but also may facilitate the study of many fields related to the polymer materials.

Here, this review focuses on feasible strategies based on chemical structure design and synthesis, which can radically alter bulk properties, to improve the triboelectric property of triboelectric polymers. The relationship between the chemical structure of polymers on the nanoscale and their electrification capability on the macroscale is also discussed. Advanced triboelectric polymers, including high charge density negative/positive triboelectric polymers, covalent organic frameworks (COFs), adjustable copolymers and robust composite materials, are provided. Strategies, mechanisms and experimental conclusions that can inspire and guide the future research on the design, synthesis and preparation of high-performance triboelectric polymers are also summarized. Finally, the challenges and prospects of the development of triboelectric polymers for high performance TENGs are outlined.

## 2. The basic principle of TENGs

TENGs are an emerging micro–nano energy harvesting technology that leverages the coupling effect of triboelectrification and electrostatic induction.<sup>53</sup> The four basic working modes of TENGs, including the contact-separation mode, lateral sliding mode, single-electrode mode, and free-standing mode, can evolve into complex structures for diverse applications.<sup>54</sup> Taking the vertical contact-separation mode TENG as an example, two pieces of dielectric material with conductive back electrodes are assembled together with an external circuit and load, as shown in Fig. 1a. During two tribo-layers contacting under the driven of external mechanical forces, contact electrification occurs and two opposite

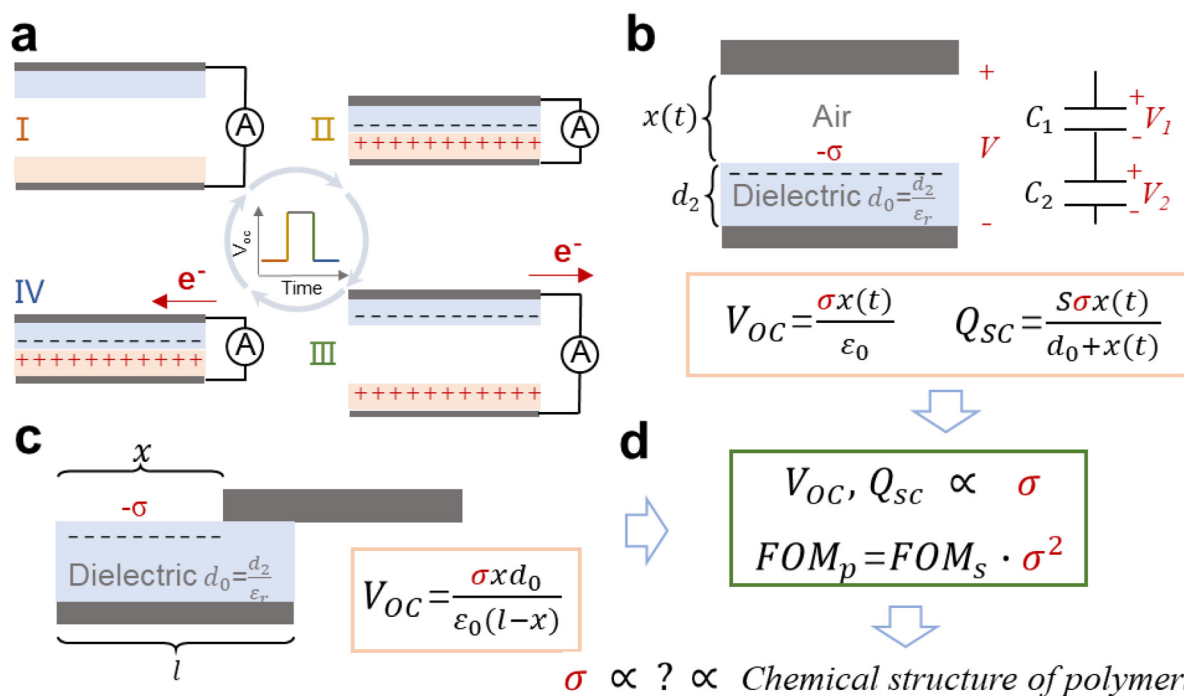


Fig. 1 (a) The basic mechanism of the vertical contact-separation mode TENG based on a double dielectric tribo-layer. (b) The theoretical model of the vertical contact-separation mode TENG based on a dielectric and conductive tribo-layer, and its equivalent circuit diagram. (c) The theoretical model of the lateral-sliding mode TENG and figure of merits (d) related to the surface charge density.

electrostatic charges generate on the surface of the dielectric material (II in Fig. 1a),<sup>55</sup> while the flow of electrons in the external circuit compensates the charge balance and generates a displacement current, which is the electrostatic induction effect. Similarly, a reverse current pulse occurs when the two tribo-layers separate (III in Fig. 1a). Cycling through this contact-separation process, a continuous flow of alternating current electrical signals is generated and the load can be driven.

The power generation principle of contact-separation mode TENGs can be deduced by a planar plane capacitance model, as shown in the simplified dielectric-metal TENG (Fig. 1b).<sup>56</sup> As the electrons flow between the two electrodes, the nanogenerator acts like a capacitor consisting of a polymer capacitor and a variable air capacitor. The voltage of the 'capacitor' drives electrons to flow through the external circuit and run the load, which can be calculated as follows:

$$V = -\frac{Q}{S\epsilon_0} \left( \frac{d_2}{\epsilon_{r2}} + x(t) \right) + \frac{\sigma x(t)}{\epsilon_0} \quad (1)$$

where  $Q$  represents the transferred charges between two electrodes, and  $\sigma$  is the surface charge density of the tribo-layer. There is no correlation between dielectric constant and triboelectric capacity by comparing the ranking in the triboelectric series with the dielectric constant.<sup>57</sup> The sum of the ratio of dielectric material thickness to its relative permittivity is defined as the effective thickness constant:

$$d_0 = \sum \frac{d_i}{\epsilon_{ri}} \quad (2)$$

Then, the voltage of the TENG can be given as

$$V = -\frac{Q}{S\epsilon_0} (d_0 + x(t)) + \frac{\sigma x(t)}{\epsilon_0} \quad (3)$$

Therefore, the open-circuit voltage and maximum short-circuit transferred charge are proportional to the surface charge density  $\sigma$ :

$$V_{oc} = \frac{\sigma x(t)}{\epsilon_0} \quad (4)$$

$$Q_{oc} = \frac{S\sigma x(t)}{d_0 + x(t)} \quad (5)$$

Similarly, the open-circuit voltage of the lateral-sliding TENG (Fig. 1c) can also be obtained as follows:<sup>58</sup>

$$V_{oc} = \frac{\sigma x d_0}{\epsilon_0 (l - x)} \quad (6)$$

The same relationship that the output performance of the TENG is proportional to the surface charge density  $\sigma$  is also suitable for the lateral-sliding TENG, and other mode TENGs. Moreover, the largest possible output energy  $E_m$  of the TENG with different loads is

$$E_m = \frac{1}{2} Q_{sc,max} (V_{oc,max} + V'_{max}) \quad (7)$$

which is proportional to the square of the surface charge density.<sup>59</sup> The performance figure-of-merit (FOM<sub>p</sub>) consisting

of structure FOM<sub>s</sub> and material FOM<sub>M</sub> ( $\sigma^2$ ) is proposed to evaluate the TENG performance:

$$FOM_p = FOM_s \cdot \sigma^2 = 2\epsilon_0 \frac{E_m}{Ax_{max}} \quad (8)$$

where the structural FOMs are only related to the mechanical structure and working mode of the TENG without materials' properties:

$$FOM_s = \frac{2\epsilon_0}{\sigma^2} \frac{E_m}{Ax_{max}} \quad (9)$$

Therefore, the maximum surface charge density determined by the chemical structure and energy band structure is a material property that directly affects the output performance of the TENG (Fig. 1c and d). It is also the basis for quantitative ranking of triboelectric properties of polymers in the triboelectric series. The triboelectric property of polymers, in particular, the influence factor on the charge density, is fundamental for the output performance of TENGs.

### 3. The relationship between chemical structure and triboelectric properties

The electrical properties of polymers, including dielectric properties under alternating electric fields, conductive properties under weak electric fields, breakdown properties under strong electric fields and electrostatic phenomenon on polymer surfaces, are closely related to their chemical structure. Among them, the electrostatic phenomenon on the polymer surface discovered before 1600 has played an important role in the discovery and exploration of electrostatics and electric charges. This process is a particularly complex process involving complex physical and chemical process mechanisms<sup>60-63</sup> and being affected by the experimental conditions such as pressure,<sup>64,65</sup> temperature,<sup>66,67</sup> humidity,<sup>68</sup> sample roughness,<sup>69,70</sup> *etc.* Research on the origin and physics of electric charge,<sup>71</sup> application of electrostatic printers,<sup>72</sup> KPFM technology<sup>73,74</sup> and electrostatic catalysis<sup>75-77</sup> has promoted the research of polymer triboelectrification to some extent. However, the triboelectric properties of polymers are still mysterious and unpredictable, due to the lack of research drive.<sup>78</sup> In particular, the relationship between the chemical structure of polymers on the nanoscale and their electrification capability on the macroscale is ambiguous and uncertain. To quantify the triboelectric property of materials, a triboelectric series that arranges triboelectric materials by their polarity and surface charge density is proposed. The first triboelectric series includes only a few materials, which is published by Wilke in 1757.<sup>71,79</sup> With the development of materials and continuous enrichment, the variety of materials in the triboelectric series is also increasing and common types of polymers are also included.<sup>80</sup> The semi-quantitative tribo-electric series for polymeric materials is proposed by A. F. Diaz.<sup>81</sup> After TENGs were proposed, the emergence and development of TENGs greatly promotes the research and application of triboelectric polymers. A standardized triboelectric series ranking over 50 polymers by the TENG output based on tested polymers with liquid metal Hg under well-defined

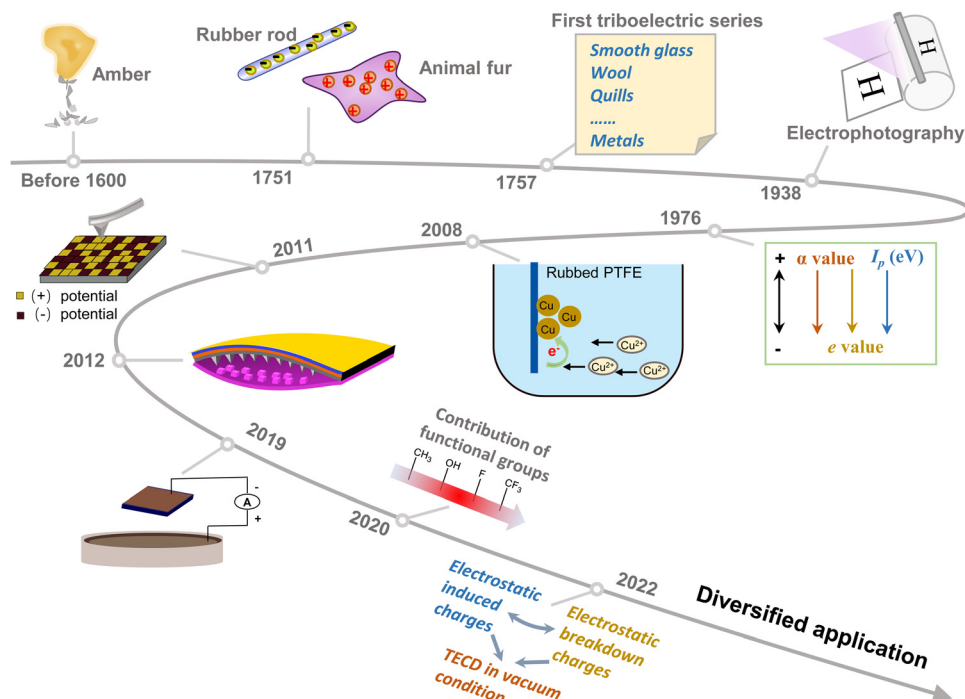


Fig. 2 The timeline of the development of electronification and triboelectric polymers.

conditions is measured.<sup>82</sup> The contributions of different functional groups of triboelectric polymers to their charge density and polarity are recognized and proposed.<sup>83</sup> Moreover, a material's intrinsic triboelectric charge density is measured under high vacuum, to suppress the electrostatic breakdown that greatly reduces electrostatic charge density.<sup>60,84</sup> The timeline of major developments of triboelectric polymers is shown in Fig. 2.

The results of the triboelectric series based on experimental data can greatly help to summarize the fundamental rules.<sup>81</sup> The empirical conclusions are as follows:

- The nitrogen containing polymers possess the most positive ranking, such as polyamide (PA), polyurea and amino resin;
- The halogenated polymers including fluorinated ethylene-propylene (FEP), polytetrafluoroethylene (PTFE) and polyvinyl chloride (PVC) have excellent triboelectric negative charge properties; and
- The neutral polyolefins polyethylene (PE), polypropylene (PP) and polystyrene (PS), and oxygen-containing polymers like polyester and polyvinyl alcohol (PVA) develop almost no charge or weak triboelectric capacity.

Furthermore, the polarity of the 10 similar carbon chain polymers is proposed to correlate with the structure and property of the repeat unit (Fig. 3a). The repeat unit has a stronger Lewis basicity when  $\Delta G$  (the Gibbs energy of the reaction with the reference molecule 4-FC<sub>6</sub>H<sub>4</sub>OH, indicative of the Lewis basicity) is lower, and polymers tend to be positively charged in the triboelectric series. However, only a few polymers agree with this correlation, and its universality still needs to be verified. The output performance of the TENG based on triboelectric polymers can be used to study triboelectric properties and quantify the triboelectric charge density precisely.<sup>59</sup> A series of vinyl polymers

with different pendant groups (Fig. 3b) are also studied as triboelectric polymers.<sup>83</sup> The result indicates that the types and densities of functional groups with electron-withdrawing/donating ability in the repeat unit can determine the macroscopic electrification behaviour of the polymer. It should be noted that this is also applicable to surface chemical modifications, which have a change in functional groups and chemical structures on or near the surface, such as surface silane coupling agent treatment, surface grafting, surface reactions, *etc.*<sup>85–88</sup> Therefore, the triboelectric property of the polymer is determined by its chemical structure, or the repeat unit property is determined by the monomer structure in other words.

A uniform intrinsic parameter of the chemical structure is desired to elucidate the relationship between the polymer structure and triboelectric properties, which can guide the design and development of triboelectric polymers. Previous studies have proposed different physical properties for explaining this relationship, such as the work function,<sup>57,89</sup> electron affinities,<sup>90</sup> energy levels of the molecular orbitals,<sup>91,92</sup> ionization potential,<sup>93,94</sup> interfacial barrier,<sup>95</sup> the Lewis basicity,<sup>81,96</sup> intermolecular forces,<sup>97,98</sup> *etc.* However, only a few polymers fit these correlations, and theories that are universal in all polymerizations are still needed. The electron affinity (EA) and the ionization potential, which is closely linked with the chemical structure of molecular, can guide the design and synthesis of high-performance triboelectric polymers since it indicates the change in energy of gaining or losing an electron to become an ion. The electron affinity is defined as the change in energy when a neutral molecule (ground state) gains an electron and becomes  $-1$  ion, which includes vertical electron affinity and adiabatic electron affinity (Fig. 3c). The polymers with a large electron affinity (EA) value, such as the polymers containing

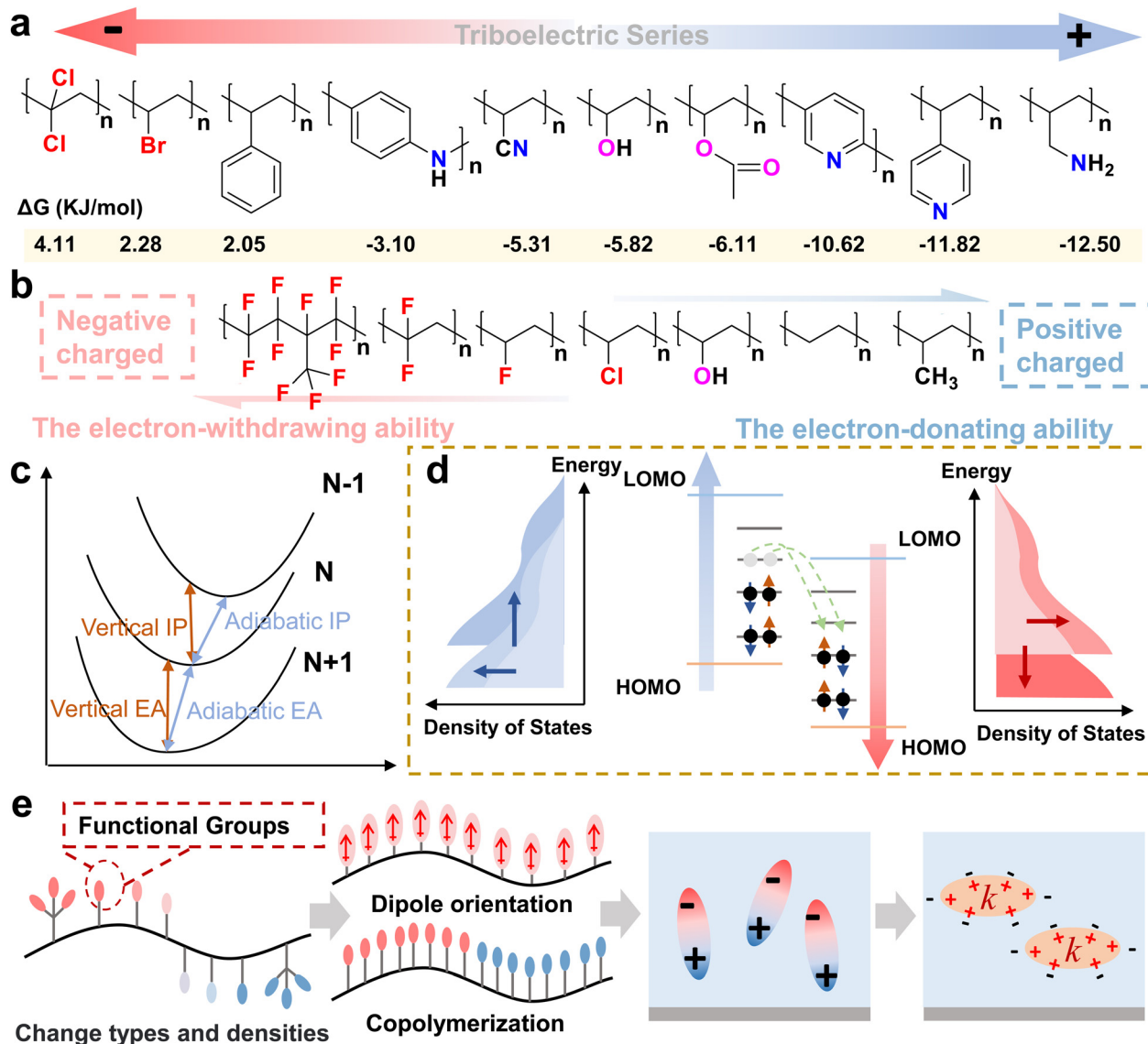


**Fig. 3** (a) The correlation between the Lewis acidity/basicity of the repeat unit of the 10 selected polymers and the ranking in the triboelectric series.  $\Delta G$  is the Gibbs energy of the reaction with the reference molecule 4-FC<sub>6</sub>H<sub>4</sub>OH, indicative of the Lewis basicity. (b) A series of vinyl polymers with different pendant groups and their electron-withdrawing/donating ability agreeing with the triboelectric property of polymers. (c) Schematic diagram of the electron affinity and the ionization potential. (d) Sketch map of the energy levels of the molecular orbitals for high performance triboelectric negative/positive polymers. (e) Schematic diagram of the strategy to improve the triboelectric property of polymers: change the types and density of functional groups in the polymer chain; adjust the orientation of pendant groups with intrinsic dipoles and copolymerization; enhance the dipole effect in the polar polymer; introduction of an interface by doping and compositing with fillers.

halogen elements (EA =  $-270$  to  $-349$  kJ mol<sup>-1</sup>), usually tend to have an excellent negative triboelectric property.<sup>99</sup> The ionization potential (IP) is the change in energy when a neutral molecule (ground state) loses an electron and becomes +1 ion, which includes vertical ionization potential and ionization potential (Fig. 3c). This value may contribute to the positive triboelectric property of the material. The work function is the energy difference between the vacuum level and the Fermi level, which is the energy barrier for an electron escaping from the surface of a material. The work function can also be used to characterize a material's ability to possess and capture electrons, and has been reported to be strongly related to the triboelectric property of the material.<sup>57</sup> Moreover, the energy

band structure, including the highest occupied atomic orbital (HOMO), lowest unoccupied molecular orbital (LOMO) and defect states in the gap (Fig. 3d), is more comprehensively explained the mechanism of triboelectric properties determined by polymer characteristics, especially the effect of crystallization, defects and other changes on the triboelectrification of the polymer. The negative/positive polarity of triboelectric polymers acquires a low LOMO level and high HOMO level, respectively. High density of defect states and charge trap in the gap contribute to the transferred charge density and charge stability. Combining the above principle, the approach and strategies to find or design high performance triboelectric polymers have some guidance and direction.

Recently, air breakdown that occurs on the surface of triboelectric polymers has also been realized as the reason limiting the high charge density.<sup>17</sup> In a vacuum, air breakdown is suppressed, and the charge density is greatly increased, and a triboelectric series under vacuum has been reported.<sup>84</sup> On the other hand, air breakdown can also be exploited for direct-current TENGs,<sup>10,17,100</sup> and fast surface charge injection techniques<sup>101</sup> to improve energy harvesting efficiency. However, the intrinsic triboelectric polarity and triboelectric characteristics of the polymers are not affected, which is related to the chemical structure and properties.

There are generally two ways to modify the triboelectric property of polymers: surface modification or synthesis and fabrication of polymers. Compared with surface modification,<sup>102,103</sup> synthesis and fabrication of polymers can change triboelectric properties at the bulk level with durability and stability. The strategies are as follows:

(1) Changing functional groups by designing or selecting monomers used for polymerization. Abundant available kinds of monomers with a wide range of possible designs are still a promising method to synthesize novel triboelectric polymers and superior negative/positive polymers beyond existing commercial polymers.

(2) Adjusting the conformation of the pendant group with intrinsic dipoles. By matching the directions of electric field or increasing the crystalline process (annealing confined crystallization) to orient dipoles as possible, the polarity of triboelectric polymers can be enhanced and the output current have boosted increase.<sup>104</sup>

(3) Copolymerization or blending can integrate multiple units or polymers with different properties to obtain performance improvement and functional advantage.

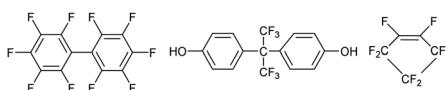
(4) Introduction of inorganic fillers and ionic electrolytes to form nanocomposites, which cause interfacial polarization and more charge trap in the gap, can increase the triboelectric charge density of polymers.

## 4. The detailed strategy for design and synthesis of triboelectric polymers

### 4.1 Advances in excellent negative triboelectric polymers

By selecting two polymers as far as possible in the triboelectric series as tribo-layer pair materials, a considerable TENG output can be obtained. Therefore, designing or finding superior negative polymers is of great significance to enhance the

**Table 1** Chemical structures and triboelectric performance of available fluoropolymers

Abbr.	Chemical structure
PFA	$\text{-(CF}_2\text{-CF}_2\text{)}_n\text{-(CF}_2\text{-CF)}_m\text{-}$ $\text{OCF}_2\text{CF}_2\text{CF}_3$
FEP	$\text{-(CF}_2\text{-CF}_2\text{)}_n\text{-(CF}_2\text{-CF)}_m\text{-}$ $\text{CF}_3$
PTFE	$\text{-(CF}_2\text{-CF}_2\text{)}_n\text{-}$
PCTFE	$\text{-(CF-CF}_2\text{)}_n\text{-}$ $\text{Cl}$
P(VDF-HFP)	$\text{-(CH}_2\text{-CF}_2\text{)}_n\text{-(CF}_2\text{-CF)}_m\text{-}$ $\text{CF}_3$
P(VDF-TFE)	$\text{-(CH}_2\text{-CF}_2\text{)}_n\text{-(CF}_2\text{-CF}_2\text{)}_m\text{-}$
P(VDF-TrFE)	$\text{-(CH}_2\text{-CF}_2\text{)}_n\text{-(CF}_2\text{-CHF)}_m\text{-}$
PVDF	$\text{-(CH}_2\text{-CF}_2\text{)}_n\text{-}$
ETFE	$\text{-(CH}_2\text{-CH}_2\text{)}_n\text{-(CF}_2\text{-CF}_2\text{)}_m\text{-}$
PVF	$\text{-(CHF-CF}_2\text{)}_n\text{-}$
THV	$\text{-(CF}_2\text{-CF}_2\text{)}_n\text{-(CF}_2\text{-CF)}_m\text{-(CH}_2\text{-CF}_2\text{)}_p\text{-}$ $\text{CF}_3$
Cytop <sup>®</sup>	$\text{-(CF}_2\text{-CF-CF-CF}_2\text{)}_n\text{-}$ $\text{O}$ $\text{CF}_2$
Teflon <sup>®</sup> AF	$\text{-(CF-CF)}_n\text{-(CF}_2\text{-CF)}_m\text{-}$ $\text{O}$ $\text{CF}_2$ $\text{CF}_2$
Hyflon <sup>®</sup> AD	$\text{-(CF-C)}_n\text{-(CF}_2\text{-CF)}_m\text{-}$ $\text{OCF}_3$ $\text{O}$ $\text{CF}_2$ $\text{CF}_3$
Other fluorinated blocks	

performance of TENGs. The commonly used negative materials are mainly high fluorine-containing polymers, such as polyfluoroalkoxy (PFA), FEP and PTFE. Because of the strong electron-withdrawing ability and the high electronegativity of F element, fluoropolymers have the largest electron affinity ( $EA = -322 \text{ kJ mol}^{-1}$ ), excellent negative polarity and high charge density. Moreover, their low surface energy and excellent hydrophobicity make them a popular choice for solid-liquid TENGs.<sup>105,106</sup> A series of fluoropolymers and their copolymers have been commercialized and are available in Table 1.<sup>107</sup> The density of F atoms in the chemical structure of vinyl polymers causes the difference in polarity and surface charge density during polymer-polymer and polymer-liquid mode TENG (FEP > PTFE > PVDF > PE).<sup>83</sup> In addition, the unsaturated groups on the PTFE molecular chain generated by sputtering technology have stronger electron-withdrawing ability and higher charge density than saturated PTFE. The unsaturated C=C bonds on the main chain can enhance the electronegativity and electrostatic energy of the polymer, which can be seen in electrostatic potential simulation in Fig. 4a.<sup>83,108</sup>

For further design and preparation of an extremely negative triboelectric polymer, J. H. Lee *et al.* first designed and fabricated a fluorinated poly(*S-r*-DIB) copolymer film with a sulfur backbone (Fig. 4b).<sup>99</sup> Compared with the carbon ( $EA = -122 \text{ kJ mol}^{-1}$ ) backbone, sulfur element has high electron affinity ( $EA = -200 \text{ kJ mol}^{-1}$ ) and more coordination to bond with fluorine. The change of the backbone and increase of functional group density contribute to strong electron-withdrawing ability and outstanding triboelectric properties. The output voltage and

current of the TENG based on the fluorine poly(*S-r*-DIB) film have a 6-fold and 3-fold increase compared with commercial PTFE film, respectively. Furthermore, a blending film based on poly(*S-r*-DIB) and fluorine-rich poly(2,3,4,5,6-pentafluorostyrene) (PPFS) directly is proposed to avoid toxic gases generated during the fluorination process (Fig. 4c).<sup>109</sup> The hydrophobic PPFS generates phase separation and subsequently migrates to the polymer air interface during hot-press forming, resulting in hydrophobicity and high surface charge density of the poly(*S-r*-DIB)/PPFS blending film. The output voltage and current of the TENG also have an 8-fold and 9-fold increase compared with commercial PTFE film, respectively. Ladder-like structured polysilsesquioxane (LPEFSQs) as a hard triboelectric polymer is also proposed (Fig. 4d),<sup>110</sup> which can be coated easily on various substrates. This hard coating exhibits excellent processability, negative polarity (more negative than PTFE) and superior mechanical properties, which is promising for the actual perpetration and application of TENGs. Poly(1*H*,1*H*,2*H*,2*H*-perfluorodecyl methacrylate) (PFDMA) with a low surface energy and highly negative triboelectric properties is also reported as an outstanding triboelectric polymer (Fig. 4e).<sup>111</sup> The repeating unit has a fluorinated long alkyl chain with strong electron-withdrawing ability, which can be used to transfer a special surface micro-nano structure to enhance the TENG performance. An amorphous fluoropolymer such as perfluoro(1-butenyl vinyl ether) (Cytot<sup>®</sup>, AGC) with transparency, hydrophobicity and negative triboelectric property is a qualified candidate for liquid-solid TENGs (Fig. 4f). Similar fluoropolymers based on perfluorocyclopentene and 4,5-difluoro-2,2-bis(trifluoromethyl)-1,3-dioxole (PDD) monomer are

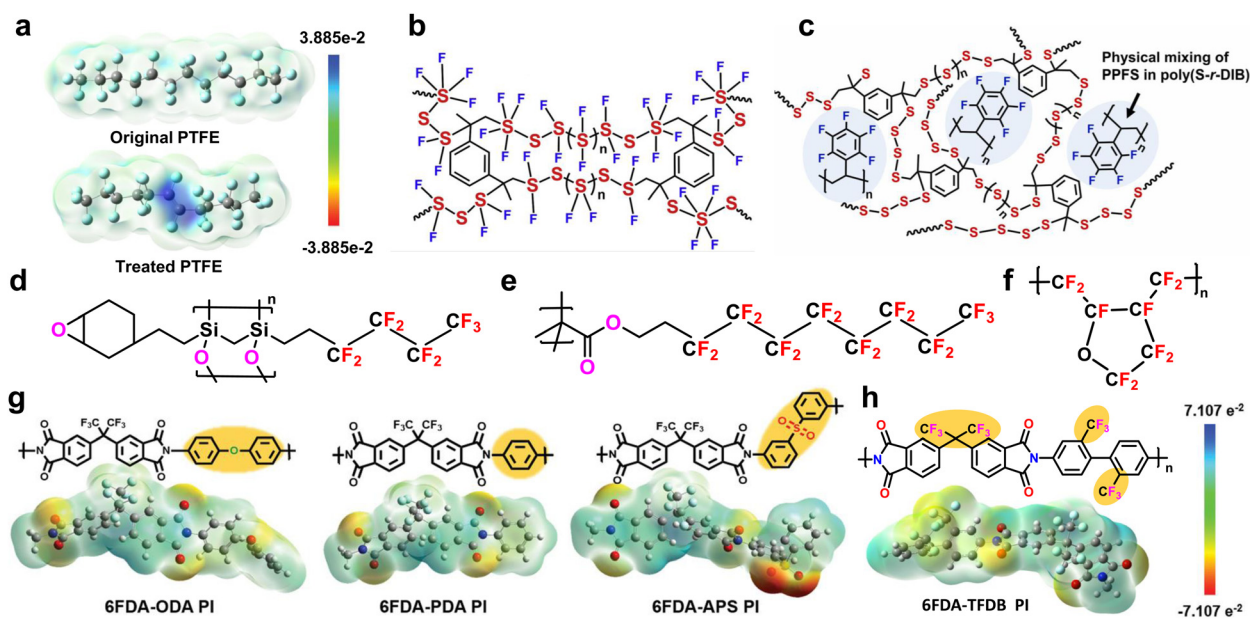


Fig. 4 (a). Electrostatic potential simulation of pristine  $C_{12}F_{26}$  (simulating PTFE) and sputtering treated PTFE with unsaturated C=C bonds. Reproduced with permission from ref. 108, Copyright 2022, Wiley-VCH. Chemical structure of fluorine poly(*S-r*-DIB) (b) and poly(*S-r*-DIB) mixes with fluorine-rich poly(2,3,4,5,6-pentafluorostyrene) (PPFS) (c). Reproduced with permission from ref. 99, Copyright 2019, Elsevier and ref. 109, Copyright 2021, Elsevier, respectively. Chemical structure of ladder-like structured polysilsesquioxane (LPEFSQs) (d), PFDMA (e) and perfluoro(1-butenyl vinyl ether) (Cytot<sup>®</sup>, AGC) (f). Chemical structure and 3D electrostatic potential simulation of synthetic PI: 6FDA-APS PI (g) and 6FDA-TFDB PI (h). Reproduced with permission from ref. 114, Copyright 2019, WILEY-VCH and ref. 115 Copyright 2019, WILEY-VCH.

also promising negative triboelectric polymers for achieving high performance.<sup>112,113</sup>

For polycondensation polymers, a variety of fluorinated monomers can be used to design and synthesize remarkable negative polymers with good mechanical properties. For example, polyimide (PI) is a kind of engineering plastic with high modulus, high strength and heat resistance, having hundreds of diamines and dianhydrides to choose for synthesis. J. M. Baik *et al.* electrostatic potential (Fig. 4g) and lower LUMO level. The triboelectric charge density of the 6FDA-APS PI film can reach  $860 \mu\text{C m}^{-2}$  after the ion injection process, which is significantly improved (7 times) compared with commercial Kapton.<sup>114</sup> The 6FDA-TFDB PI, which contains four trifluoromethyl groups (Fig. 4h) in the repeating unit, has also been synthesized for high performance negative triboelectric polymers.<sup>115,116</sup> Moreover, fluorinated PIs exhibit an excellent transparency property and can be selected for TENGs where transparent and flexible tribo-layers are required. Other polycondensate polymers such as polyester, polysulfone, and polyether also have broad potential to be designed and synthesized as high-performance triboelectric polymers.

#### 4.2 Advances in positive triboelectric polymers

Positive triboelectric polymers, represented by polyamide (PA), epoxy resin and amino resin, have the advantages of flexibility, stretchability, processability, low cost, *etc.* compared with stiff, brittle metal and inorganic positive materials for flexible, large-scale TENGs. However, there are fewer options and the research is still insufficient. From the triboelectric series and experimental conclusion, it is found that polymers containing NH and unsaturated N groups usually have an excellent positive triboelectric property. In this respect, butylated melamine

formaldehyde (BMF) with long alkyl chains and unsaturated N groups is synthesized as a triboelectric polymer for rotation-type TENGs.<sup>117</sup> Since the electron-donating ability of functional group, BMF has increased HOMO states (Fig. 5a) and then more positive than pristine MF and methylated MF. Meanwhile, mechanical durability and hardness are also obtained to satisfy the long-term continuous friction. The TENG based on the BMF tribo-layer can achieve  $24 \text{ mA m}^{-2}$  current density, and retain stable output over 27 000 cycles. Functional groups can also be designed on the end group to achieve functional purposes and positive polarity. For example, a series of telechelic elastomers with hierarchical hydrogen-bond (H-bonds) networks constructed by 2-ureido-4 pyrimidinone and urea groups are designed.<sup>118</sup> The reversible dynamic network formed by abundant NH groups at the chain end (Fig. 5b) gives the elastomer a more positive triboelectric property than PA, as well as high stiffness, high adhesion strength and interesting aggregation induced emission fluorescence. In addition, non-bonding electrons in nitrogen-based polymers are proposed that can contribute to creating an electron-donating environment and enhance the positive triboelectric property. To maximize the number of non-bonding electrons with local dipoles nitrogen-based dimethylol urea (DMU), diazolidinyl urea (DU), and imidazolidinyl urea (IU) are designed and synthesized as promising positive triboelectric materials.<sup>119</sup> The smaller HOMO distributions of IU because of the non-bonding electrons in O and N, forming more donating electrons around the Fermi energy with the strongest negative local dipole, can be seen in calculated results (Fig. 5c). IU exhibits 8.7 times higher current density ( $42.11 \text{ mA m}^{-2}$ ) than positive nylon ( $4.79 \text{ mA m}^{-2}$ ) during contact with PTFE (Fig. 5d). A biobased polyamide

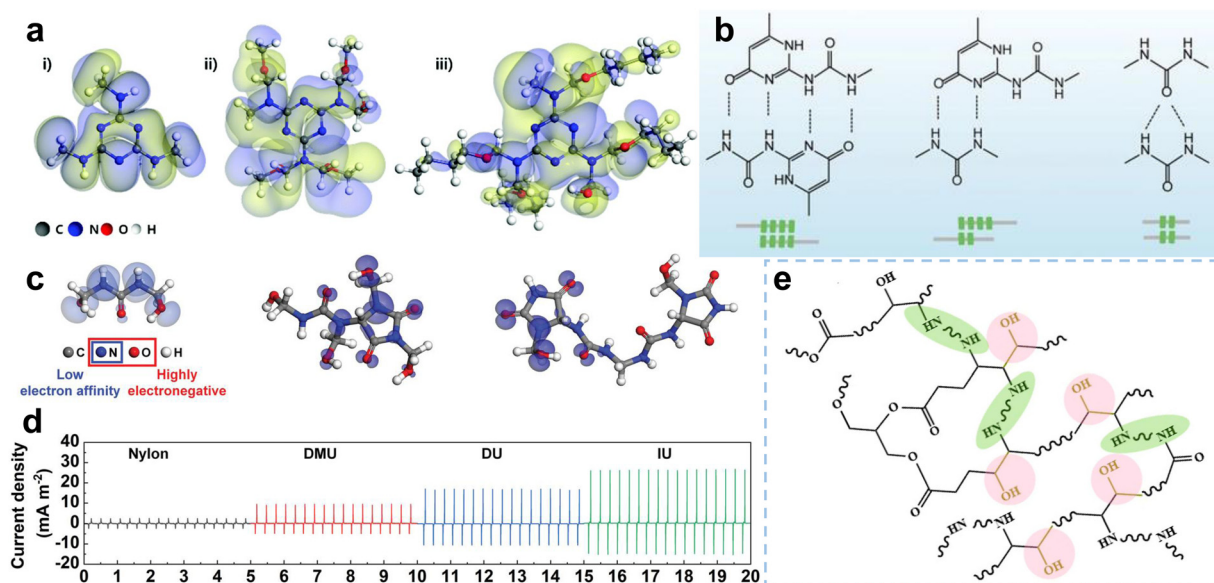


Fig. 5 (a). The distribution of HOMO states of pristine MF, methylated MF and BMF. Reproduced with permission from ref. 117, Copyright 2019, The Royal Society of Chemistry. (b). The quadruple and double H-bonds constructed in the telechelic polymers, respectively. Reproduced with permission from ref. 118, Copyright 2022, Wiley-VCH. (c). The chemical structures and calculated HOMO distribution of DMU, DU, and IU, respectively. (d). Triboelectric current density of nylon, DMU, DU, and IU during contact with PTFE, respectively. Reproduced with permission from ref. 119, Copyright 2022, Wiley-VCH. (e). The chemical structure of crosslinked biobased polyamide. Reproduced with permission from ref. 120, Copyright 2022, American Chemical Society.



synthesized through the crosslinking of epoxidized soybean oil with hexamethylenediamine (HMDA) is designed (Fig. 5e), which contains many NH amide structures.<sup>120</sup> This polyamide film has an outstanding positive triboelectric property, and the polarity is related to the content of the N-containing crosslinking agent HMDA. Using biomass materials instead of petroleum-based products is a low-cost, environmentally friendly and sustainable strategy. Other polymers such as cellulose and its derivatives,<sup>121,122</sup> epoxy resin,<sup>123,124</sup> and rubber and its modified polymers<sup>125–127</sup> have been also proposed as promising positive triboelectric polymers, and have a wide development prospect. Positive polymers have incomparable flexible advantages compared with inorganic and metal materials, but the polarity still needs further development.

#### 4.3 Covalent organic frameworks (COFs) as triboelectric polymers

Covalent organic frameworks (COFs) are an advanced class of crystalline porous materials that possess unique architectures,

high surface areas and tuneable pore sizes.<sup>128,129</sup> The diversity and designable periodic two-dimensional (2D) and three-dimensional (3D) structures endow COFs with outstanding performance in electrochemical energy storage and conversion,<sup>130,131</sup> gas separation and purification,<sup>132,133</sup> heterogeneous catalysis,<sup>134</sup> and proton-conductive membranes.<sup>135</sup> The advantages of periodic conjugate structure and functional group design may also enable COFs as excellent triboelectric polymers. In this area, a series of COFs with designable skeletons and functional groups are synthesized to attempt as triboelectric polymers by Lipeng Zhai *et al.*<sup>136–138</sup> A bromine functionalized TPB-DBBA-COF is synthesized from the linker 2,5-dibromobenzene-1,4-dicarbaldehyde (DBBA) and knot 1,3,5-tris(4-aminophenyl) benzene (TPB) (Fig. 6a).<sup>138</sup> The TPB-DBBA-COF possesses similar positive triboelectric polarity to PA6 and attains high charge density ( $51.2 \mu\text{C m}^{-2}$  at 5 Hz contacting with PVDF). This property is attributed to its larger surface area, better crystals and bromine groups with charge

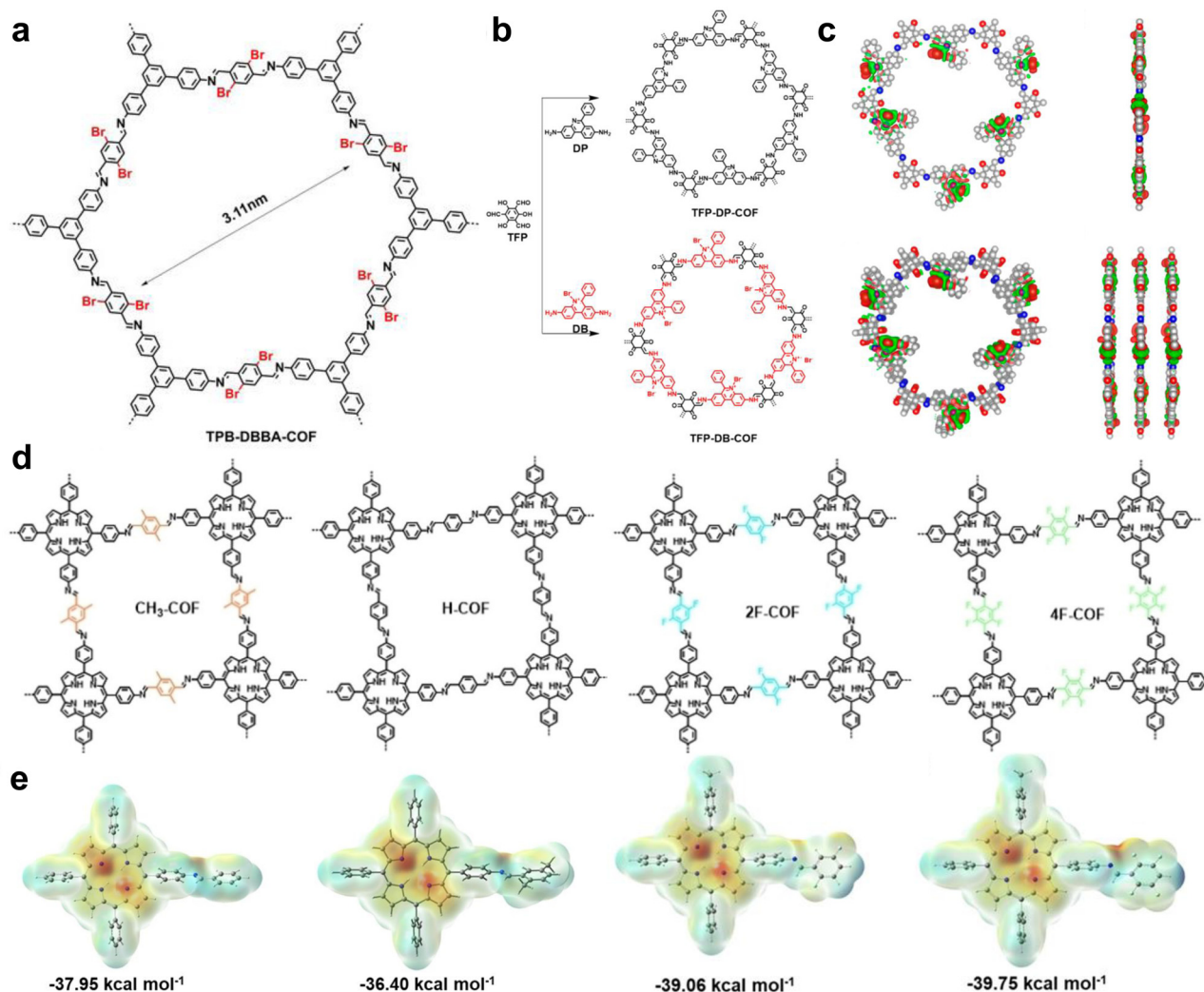


**Fig. 6** (a) Chemical structure of TPB-DBBA-COF. Reproduced with permission from ref. 138, Copyright 2020, Wiley-VCH. (b) Schematic of the synthesis of TFP-DP-COF and cationic TFP-DB-COF, and their simulated different charge states (c). Reproduced with permission from ref. 136, Copyright 2020, American Chemical Society. (d) Chemical structure of 2D porphyrin COFs with tunable functionalities ( $\text{CH}_3$ , H, 2F, and 4F). (e) Simulated electrostatic potential distribution and electron affinity of porphyrin COFs. Reproduced with permission from ref. 137, Copyright 2020, Wiley-VCH.

delocalization effect. A triazine skeletal nitrogen-rich COF with highly positive polarity and abundant conjugated structure is also reported as a triboelectric polymer.<sup>139</sup> A novel fluorinated COF based on 1,3,5-tris(2,3,5,6-tetrafluoroaniline) benzene (TFAB) and trimethylphloroglucinol (Tp) is combined with PVA to form a positive tribo-layer for high performance TENGs.<sup>140</sup> Furthermore, a cationic TFP-DB-COF based on the 1,3,5-trimethylphloroglucinol (TFP) knot and dimidium bromide (DB) linker is proposed, with cationic groups exposed to the channel surface (Fig. 6b).<sup>136</sup> The different charge state caused by cationic groups can increase charge density ( $73.5 \mu\text{C m}^{-2}$ ) and charge transport capacity compared with neutral TFP-DP-COF, as shown in the simulated charge density difference (Fig. 6c). Introduction of cationic groups in skeletons is an effective method to further improve charge generation and charge transport of COFs for high charge density TENG devices. COFs with excellent designability can also be used to synthesize negative polymers by selecting various functional groups. A series of porphyrin-based COFs with  $\text{CH}_3$ -, H-, 2F- and 4F-groups are designed (Fig. 6d), and then composited as fillers in PVDF as a tribo-layer.<sup>137</sup> With the strong electron-withdrawing ability of 4F-groups, 4F-COF has increased charge-trapping sites and electron affinity (Fig. 6e), and consequently has the most negative property and maximum power density ( $2858 \text{ mW m}^{-2}$ )

compared with other COFs. Considerable progress has been made in COF triboelectric polymers; however, there are still huge challenges in fabricating COF films for TENGs. Mature film forming and processing methods such as large area film growth or composite with another polymer are required for achieving robust and durable triboelectric polymers.

#### 4.4 Adjustable copolymers for TENGs

Copolymerization is usually an effective strategy to adjust and enhance properties by integrating the advantages of two or multiple polymers. This strategy can also be applied to control the triboelectric property, and even bring functional features for triboelectric polymers. The commonly used FEP and PFA with outstanding negative triboelectric properties are copolymers of tetrafluoroethylene and perfluoropropylene and perfluorooxyethylene, respectively. Those PTFE-based copolymers have higher charge density and better melt-processable properties compared to PTFE. In this way, a copolymer is synthesized by free radical polymerization of negative units 3,3,4,4,5,5,6,6,7,7,8,8,9,9,10, 10,10-heptafluorodecyl methacrylate (HDFDM) and positive units poly(ethylene glycol) diacrylate (PEGDA) to regulate charge accumulation on the polymer surface (Fig. 7a).<sup>141</sup> The charge density on the copolymer surface varies approximately linearly

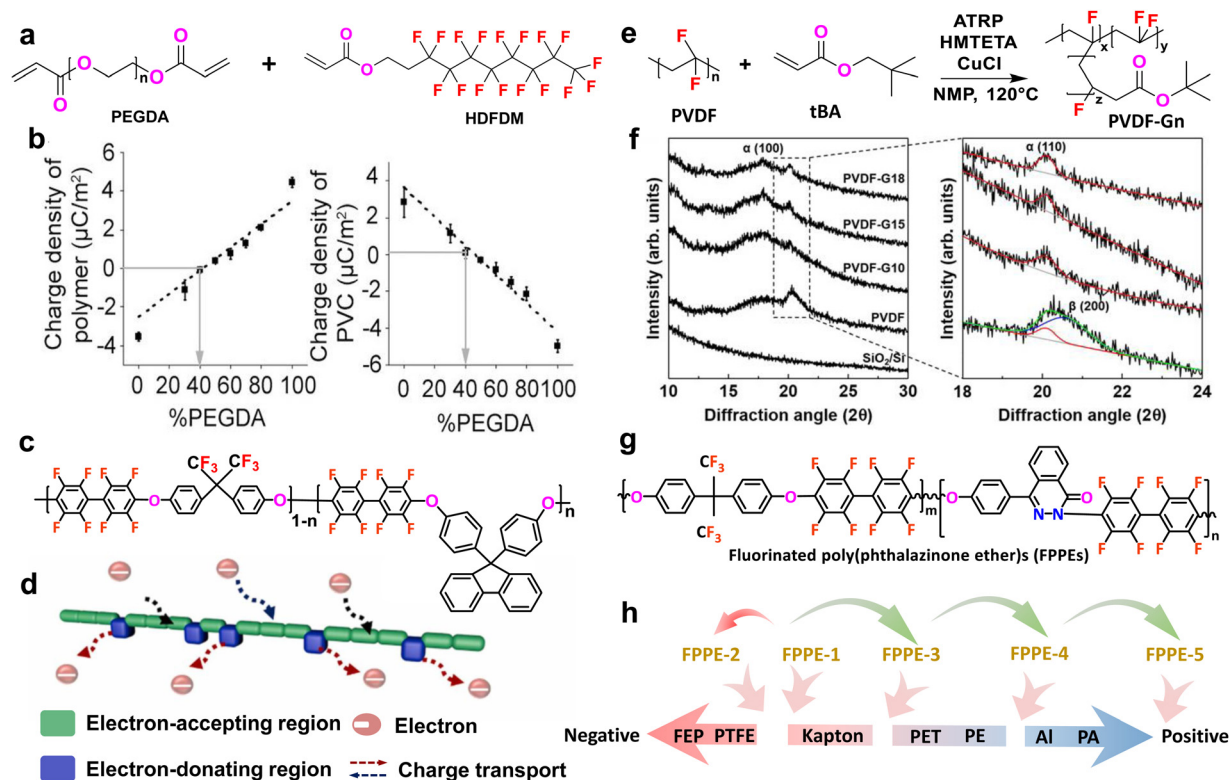


Fig. 7 (a) Chemical structure of PEGDA and HDFDM. (b) The charge density of the copolymers with different proportions of PEGDA and HDFDM and PVC as counter materials. Reproduced with permission from ref. 141, Copyright 2016, WILEY-VCH. (c) The chemical composition of fluorinated poly(arylene ether)s. (d) Schematic illustration of electronic transmission in the fluorinated poly(arylene ether)s during electrification. Reproduced with permission from ref. 142, Copyright 2022, Elsevier. (e) Synthesis of PVDF-Gn graft copolymers. (f) High-resolution XRD patterns and expanded view of pristine PVDF and PVDF-Gn films as a function of PtBA mole percent. Reproduced with permission from ref. 145, Copyright 2017, AAAS. (g) The chemical structure of fluorinated poly(phthalazinone ether)s. (h) The ranking of fluorinated poly(phthalazinone ether) films in the triboelectric series. Reproduced with permission from ref. 146, Copyright 2023, WILEY-VCH.

with changes in monomer ratio during contact with PVC (Fig. 7b) and other materials. A series of fluorinated poly(arylene ether)s condensed by decafluorobiphenyl and diphenol monomers bisphenol AF, and 4,4'-(9-fluorenylidene) diphenol are also proposed (Fig. 7c).<sup>142</sup> Since the introduction of  $\pi$  electrons in unsaturated groups is more likely to gain electrons,<sup>143</sup> the copolymers with 50 mol% fluorene content obtain the highest output power. The ranking in the triboelectric series also changes with the change of electron accepting and donating capabilities of the chain structure determined by monomer proportion (Fig. 7d). By controlling the ratio of monomers with the electron-withdrawing/donating groups, the chain structure of the polymers can also be adjusted to change the triboelectric properties.

Copolymerization not only changes the chain structure and functional groups, but also changes the aggregation structure and crystallization. The most representative examples are PVDF based copolymers such as P(VDF-TrFE), P(VDF-HFP) and P(VDF-TFE), which can enhance dipole orientation and crystallization by copolymerization with other monomers.<sup>107,144</sup> Similarly, poly(*tert*-butyl acrylate) (PtBA) is reported to graft into the PVDF chain by the atom-transfer radical polymerization (ATRP) technique (Fig. 7e).<sup>145</sup> The  $\beta$  phase crystal of the PVDF-based copolymer transitioned to  $\alpha$  phase with the increase of PTBA (Fig. 7f), and the dielectric constant also increased. When the percentage of PTBA reaches 18%, the current density reaches  $18.9 \mu\text{A cm}^{-2}$ , and can be further increased after polarization ( $25 \mu\text{A cm}^{-2}$ ). Increased segment regularity and crystallization may also occur during copolymerization of amorphous polymers. In this respect, 4-(4'-hydroxyphenyl)phthalazin-1(2*H*)-one (DHPZ) monomer with a non-coplanar torsional spatial structure and strong conjugated effect is proposed to introduced into co-polymerized fluorinated poly(phthalazinone ether)s (FPPEs) (Fig. 7g).<sup>146</sup> The ranking of FPPE films in the triboelectric series can be largely shifted from negative to positive by increasing conjugate phthalazinone moieties (Fig. 7h). However, FPPE-2 with 25% DHPZ has a peculiar negative shift compared to FPPE-1 without phthalazinone moieties, which is attributed to the appearance of induced crystallization. Therefore, both the molecular structure and aggregate structure can be changed during copolymerization. In brief, copolymerization is a promising strategy to adjust the triboelectric properties of polymers, but also helps to study the mechanism between the polymer structure and properties.

#### 4.5 Controlled crystallization to enhance triboelectric properties

The influence of dipole orientation and crystallization on the triboelectric properties of polymers cannot be neglected during molecular structural changes and processing processes, especially in polar polymers. For example, the crystallinity of P(VDF-TrFE) with tetrahydrofuran (THF), methyl ethyl ketone (MEK), dimethylformamide (DMF), and dimethyl sulfoxide (DMSO) solvent is different because of polymer-solvent interaction.<sup>147</sup> By using DMSO solvent, a smaller value of full width at half maximum (FWHM) of the  $\beta$  phase peak in X-ray diffraction (XRD) (Fig. 8a) and bigger melting enthalpy in differential

scanning calorimetry (DSC) (Fig. 8b) are observed compared with those using other solvents. These results indicate that high dipole alignment and crystallinity (25.59%) are obtained by using a good solvent DMSO. The output voltage of the TENG based on P(VDF-TrFE) is directly proportional to the crystal result caused by solvent selection (Fig. 8c). The control of the annealing process can determine crystallization and dipole orientation, while it can be amplified by matching the direction of electric field polarization for high performance TENGs.<sup>104,148</sup> Dipole-moment-induced effect in PVDF caused by forward-polarized, nonpolarized, and reverse-polarized is demonstrated that can substantial enhancement of the output power density of the TENG.<sup>149</sup> In addition, a nanostructured PVDF film using an immersion-precipitation method with a highly rough and porous surface is reported.<sup>150</sup> After annealing and poling at  $100^\circ\text{C}$ , the  $\alpha$ ,  $\beta$  and  $\gamma$  crystalline phases appear and the dipole aligns in electric field (Fig. 8d). The TENG based on polarised PVDF “+” with a dipole direction toward the surface has higher output voltage and current compared with PVDF “-” and non-polarised PVDF (Fig. 8e).

Confined crystallization of polymeric materials is an interesting method to generate a preferential orientation of polymeric crystals.<sup>151</sup> A gas-flow assisted nano-template (GANT) infiltration method to fabricate nylon-11 nanowires in nanoporous anodised aluminium oxide (AAO) templates is proposed (Fig. 8f).<sup>152</sup> The crystalline phase of nano-confined nylon-11 nanowires could be well-controlled using different gas flow rates at the surface. As shown in Fig. 8g, the formation and increase of the  $\delta'$ -phase ( $2\theta = 21.61^\circ$  in XRD) and decrease of the  $\alpha'$ -phase ( $2\theta = 22.61^\circ$ ) occur with the increase of gas-flow rate. The TENG based on nylon-11 nanowires has higher output voltage and current density ( $\sim 38 \text{ mA m}^{-2}$ ) during contact with Teflon film compared with Al and nylon films. Similarly, the  $\alpha$ -phase nylon-11 nanowires can also be obtained by the thermally assisted nanotemplate infiltration (TANI) method (Fig. 8h).<sup>153</sup> The intensity of the XRD peak at  $20^\circ$  and  $24.2^\circ$  representing the  $\alpha$ -phase appears when the solution concentration changes (Fig. 8i). The peak at  $24.2^\circ$  gradually decreased when dilute solution was used, indicating that slower crystallization rate and more aligned molecular structures are obtained. The  $\alpha$ -phase nylon-11 achieves higher surface potential and enhanced thermal stability, because of the ordered crystalline regions and higher molecular packing density (Fig. 8j). Therefore, the higher current density of  $\alpha$ -phase nylon-11 ( $\sim 74 \text{ mA m}^{-2}$ ), almost 3 times higher than that of the  $\delta'$ -phase, is observed. Recent reports have shown that the effect of crystallization on triboelectric properties also appears for weakly polar PCTFE<sup>154</sup> and amorphous materials,<sup>146</sup> suggesting that the effect is applicable to a wide range of polymers. Therefore, changes in crystallinity and phase during molecular synthesis,<sup>145</sup> doping, stretching,<sup>126</sup> and processing<sup>15</sup> can also cause differences in triboelectric properties of polymers. Studying and regulating the aggregate structure and crystallization is an important strategy to enhance the triboelectric properties of polymers, and also promotes the understanding of mechanisms at the higher structural level.

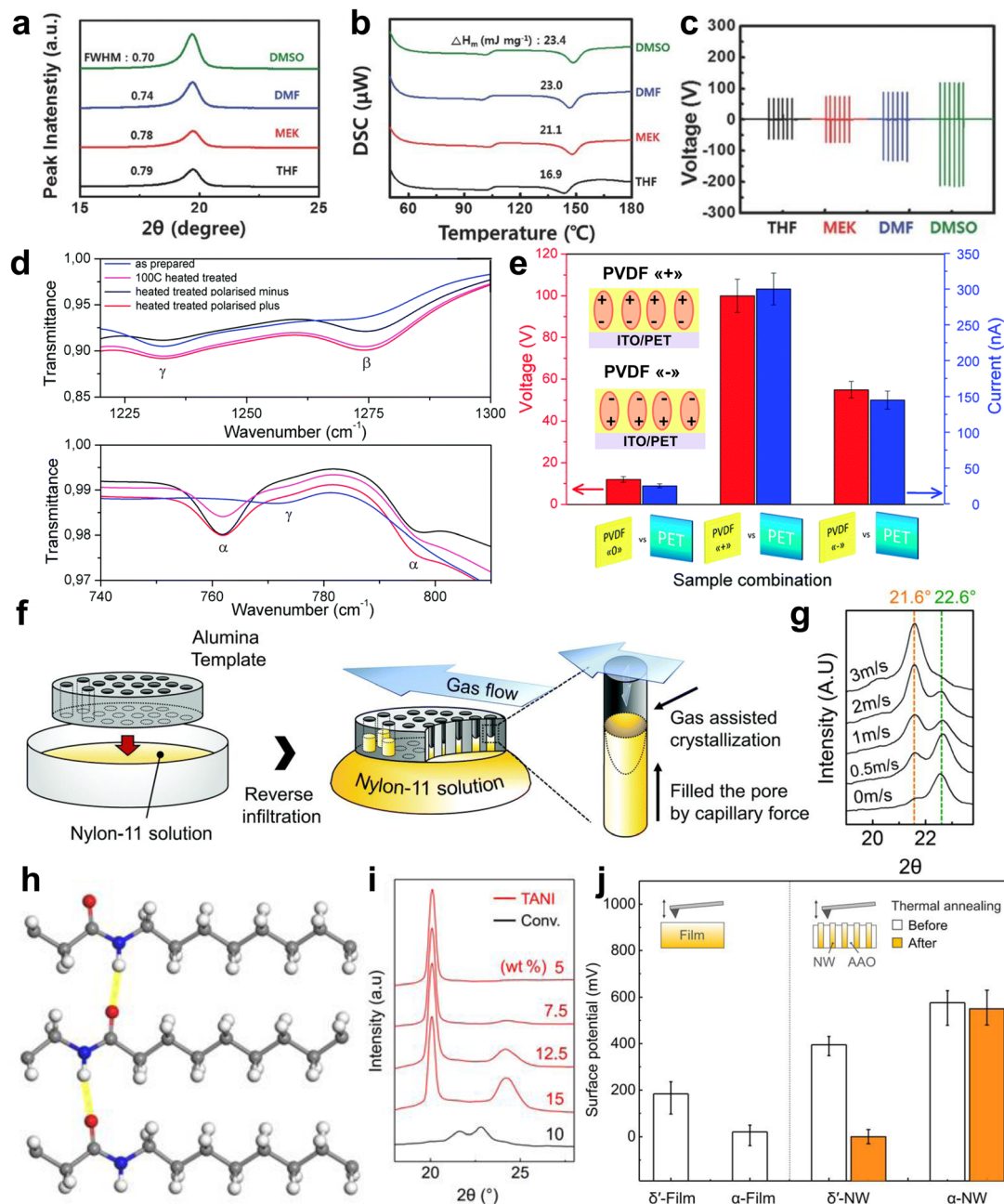


**Fig. 8** XRD measurements (a) and DSC measurements (b) of the P(VDF-TrFE) dissolved in THF, MEK, DMF, and DMSO. (c) The output voltage of the TENG based on the P(VDF-TrFE) film. Reproduced with permission from ref. 147, Copyright 2017, WILEY-VCH. (d) ATR-FTIR measurements of non-polarised PVDF, polarised PVDF "++" and PVDF "--". (e) The output voltage and current of the TENG based on non-polarised PVDF, polarised PVDF "++" and PVDF "--". Reproduced with permission from ref. 150, Copyright 2018, The Royal Society of Chemistry. (f) Schematic of the nanowire fabrication procedure by the gas-flow assisted nano-template (GANT) infiltration method. (g) XRD patterns of nanowire-filled templates crystallised at various assisted gas-flow rates. Reproduced with permission from ref. 152, Copyright 2017, The Royal Society of Chemistry. (h) Crystal structure of  $\alpha$ -phase nylon-11. (i) XRD patterns of nanowires fabricated by the conventional template-wetting (black) and the TANI (red) methods. (j) Plots of the surface potential of  $\delta'$ -phase and  $\alpha$ -phase nylon-11 nanowires, and their surface potential after 165  $^{\circ}\text{C}$  annealing. Reproduced with permission from ref. 153, Copyright 2020, AAAS.

## 5. Inorganic/organic composite materials

Compared with the homogeneous polymers, heterogeneous polymers have a large number of interfaces and defects, which can provide more charge accumulation and storage sites.

Introduction of nano-fillers moderately into the polymer matrix is a direct way to create heterogeneous interfaces and defects to enhance triboelectric properties (Fig. 9). Three types of fillers are commonly used in triboelectric polymers: (1) high dielectric constant nanoparticles with polarization characteristics can generate interface polarization and deep traps (Fig. 9b). (2)

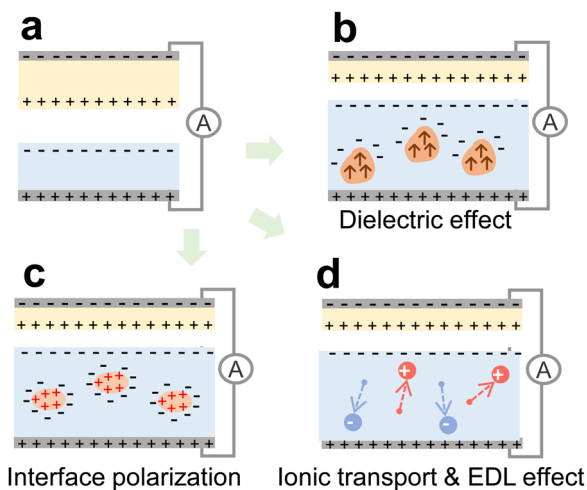


Fig. 9 Schematic diagram of the polymer film without a composite (a), and composites with dielectric nanoparticles (b), carbon-based fillers (c) and ions (d).

The introduction of carbon-based materials can produce interfaces for charge accumulation and charge confinement (Fig. 9c). (3) Ion-filler doping in ionic polymers can also affect triboelectric properties because of ion transport and migration during electrification (Fig. 9d). Here, we divide the reasons for the filler to enhance the triboelectrification ability into three aspects: dielectric effect, interface effect and double electron layer effect. In a composite film, it should be a complex system where these three effects coexist. For example, the polarization effect plays the main role, but the interface effect also exists in BTO-doped PVDF films. When the non-polarized filler changes the aggregate structure or the dipole orientation of the substrate around the filler, the polarization effect also exists. In addition to ionic electrolytes, the EDL effect is also present in composite films formed by fillers with ionized surfaces. However, superabundant fillers will destroy the insulation and dielectric strength, resulting in dielectric breakdown and limiting the triboelectric performance. Dielectric breakdown inside the material leads to a decrease in charge storage capacity. The size, shape, and property of the fillers and the dielectric properties of the substrate are closely related to the optimal content where outstanding triboelectric properties can be obtained. To achieve the balance between filler content and charge gain, an appropriate doping concentration, size and distribution of nanoparticles are required. Large concentration and poor dispersion of fillers in the polymer lead to aggregation, which contributes to the dielectric breakdown and charge leakage in composite films. A large number of in-depth studies have reported to improve triboelectric performance by nano-micro particle composites, which are summarized in Table 2.

### 5.1 High dielectric constant filler composite films

Insulating nanofillers with high dielectric constant and large specific surface area is commonly used to compensate for the polymer's low dielectric constant, which originates from electronic and atomic polarizations and is limited to 2–5.<sup>155,156</sup>

Many inorganic dielectric nanoparticles such as BaTiO<sub>3</sub>,<sup>157–159</sup> PZT,<sup>160</sup> Bi<sub>2</sub>WO<sub>6</sub>,<sup>161</sup> and SrTiO<sub>3</sub><sup>162</sup> have been proposed to improve the triboelectric charge density and polarizability. In addition, the combination of dielectric fillers and polar polymers PVDF and P(VDF-TrFE) is a promising method to prepare high performance composite films, because of the coupling of interface polarization and self-polarization effect.<sup>149,150</sup> For example, 5 wt% high dielectric BaTiO<sub>3</sub> nanoparticles are reported to composite with the P(VDF-TrFE) film, which can greatly increase interface polarization and charge trapping capability (Fig. 10a).<sup>163</sup> The difference in surface potential indicates that BaTiO<sub>3</sub> has a great improvement in charge capture and accumulation after poling (Fig. 10b). Furthermore, an alternating BaTiO<sub>3</sub>/P(VDF-TrFE) organic/inorganic multi-layer nanocomposite film is proposed to increase interfacial polarization, which has higher dielectric constant and current density than the single layer composite film (Fig. 10c).<sup>164</sup> The lamination of single- or multi-layer dielectric materials into polymer substrates has also been reported to improve the charge accumulation capacity.<sup>165–167</sup> In order to improve interface compatibility, chemical modification of the BaTiO<sub>3</sub> surface to form a core-shell-structure by a silane coupling agent and grafting PtBA is also proposed (Fig. 10d).<sup>157</sup> The dielectric/ferroelectric composite film with high relative permittivity and self-polarization effect can exploit the advantages to the full in charge pumping and excitation TENGs. Using the advantages of lead zirconate titanate (PZT) and PVDF composite film (Fig. 10e),<sup>160</sup> the dipole in the charge-excitation TENG can be quickly polarized and charge saturated under superhigh electric field (Fig. 10f). Similarly, BaTiO<sub>3</sub>/PVDF applied in the self-charge excitation TENG to enhance output performance is proposed (Fig. 10g).<sup>159</sup> In addition, some dielectric materials with a non-centrosymmetric structure and dipole orientation have been reported for use in composite films. Bismuth tungstate (Bi<sub>2</sub>WO<sub>6</sub>) with non-toxicity, high non-centrosymmetry and high dielectric constant is added in P(VDF-TrFE) to fabricate a nanocomposite fibre (Fig. 10h), which is used for TENGs and PH sensing.<sup>161</sup> Bi<sub>2</sub>WO<sub>6</sub> with a marigold flower-like structure (Fig. 10i) embedded in poly(vinylidene fluoride-co-hexafluoropropylene) (PVDF-HFP) film is also prepared, which not only results in high dielectric constant, but also increases the β-phase crystallization of the polymer.<sup>168</sup> The CaCu<sub>3</sub>Ti<sub>4</sub>O<sub>12</sub> (CCTO) particles with a cubic perovskite structure and high permittivity (up to 7500) are introduced into the positive BMF film to enhance internal polarization and output performance (Fig. 10j).<sup>169</sup> The introduction of CCTO particles is a universal strategy and also effective in PMMA, PDMS, and P(VDF-TrFE) substrates. Also, addition of other dielectric nanoparticles such as SrTiO<sub>3</sub>,<sup>162</sup> MXene,<sup>170</sup> MoS<sub>2</sub>,<sup>171</sup> BCZTBH,<sup>172</sup> and CsPbX<sub>3</sub><sup>173</sup> in the polymer matrix is proposed to improve triboelectric properties. Some magnetic or metal nanoparticles have also been reported as fillers to enhance the output performance of triboelectric polymers.<sup>174–176</sup> The doping process sequential infiltration synthesis (SIS), which can achieve deep infiltration of the inorganic compounds into certain polymers, is used to prepare composite surfaces by Yanhao Yu *et al.*<sup>177</sup> AlO<sub>x</sub> is successfully

Table 2 A list of the performance comparison of TENGs based on composite films with inorganic and carbon-based fillers and ionic electrolytes

Matrix	Filler	Counter layer	Current/charge density	Permittivity	Notes	Ref.	
PVDF	0.1 wt% BaTiO <sub>3</sub>	Sheet steel	1.67 mC m <sup>-2</sup>	~14.8	Self-charge excitation TENG	159	
	25% BaTiO <sub>3</sub>	PVDF	65.5 μC m <sup>-2</sup>	—	Inversely polarized, V-TENG <sup>a</sup>	158	
	BaTiO <sub>3</sub> -PtBA	Al	61 mA m <sup>-2</sup>	26.5	Core-shell-structured, ion injection	157	
	PZT	Stainless steel	3.53 mC m <sup>-2</sup>	26.2	Self-charge excitation TENG	160	
	MXene	PEI	66.7 mA m <sup>-2</sup>	—	7 Hz, fibrous membrane, V-TENG	170	
	rGONRs	Al	0.35V (2.5 cm × 4.5 cm)	—	Finger touching arch-shaped TENG	184	
	0.8% Active carbon	Al	51.2 mA m <sup>-2</sup> , 153.45 μC m <sup>-2</sup>	4.7	High specific surface area structure	180	
	11.3 wt% Fe <sub>3</sub> O <sub>4</sub>	Al	2.272 mA m <sup>-2</sup>	—	Electrospinning nanofiber membrane	175	
	CoFe <sub>2</sub> O <sub>4</sub>	Water	5.675 mA m <sup>-2</sup>	17.9	Liquid-solid TENG	176	
	4F-COF	PVDF	25.6 mA m <sup>-2</sup>	—	5 Hz, V-TENG	137	
	P(VDF-TrFE)	5 wt% BaTiO <sub>3</sub>	Al	333.3 mA m <sup>-2</sup> , 116.8 μC m <sup>-2</sup>	12.4	5 Hz, 6 kgf, V-TENG	165
		BaTiO <sub>3</sub> Multilayer	Al	19.2 mA m <sup>-2</sup> , 8.4 mC m <sup>-2</sup>	17.06	2 Hz, 98 kPa, V-TENG	164
	PVDF-HFP	40% Bi <sub>2</sub> WO <sub>6</sub>	Cu	11.91 mA m <sup>-2</sup>	44	1 Hz, ~0.15 kgf, nanofiber membrane	161
		2.5 wt% Bi <sub>2</sub> WO <sub>6</sub>	Cu	53 mC m <sup>-2</sup>	~9.5	Marigold flower-like structure filler	168
PDMS	AlO <sub>x</sub>	PDMS	22 mA m <sup>-2</sup> , 45 μC m <sup>-2</sup>	—	Sequential infiltration synthesis	177	
	10% BCZTBH	Al	0.56 mA m <sup>-2</sup>	—	Multi stack hybrid NG	172	
	20 wt% BaTiO <sub>3</sub>	Cu	172 mA cm <sup>-2</sup> , 69.2 uC m <sup>-2</sup>	—	Hybrid piezo/triboelectric NG	201	
	33.3% BaTiO <sub>3</sub>	Al	60.8 mA m <sup>-2</sup>	6.5	Micro-pyramid surface structure	202	
	BaTiO <sub>3</sub>	ITO	25 mA m <sup>-2</sup>	—	Sponge structure TENG	203	
	10% SrTiO <sub>3</sub>	Cu	90.6 mA m <sup>-2</sup> , 190 μC cm <sup>-2</sup>	~5	2.5 Hz, sponge structure TENG	162	
	3 wt% GPs	Al	41.25 mA m <sup>-2</sup>	2.973	2 Hz, V-TENG	204	
	CNTs	Skin	3 μA by finger tapping	—	Foam, single-electrode TENG	182	
	Aligned CNTs	PDMS	60 mA m <sup>-2</sup>	—	40 μm, arched TENG	183	
	4% CNTs-TiO <sub>2</sub>	Cu	81.48 mA m <sup>-2</sup>	—	Arched TENG	187	
	5% MOFs	Cu	92.5 mA m <sup>-2</sup> , 120 μC cm <sup>-2</sup>	3	Humidity-resistive V-TENG	205	
PI	AlO <sub>x</sub>	Kapton	56 mA m <sup>-2</sup> , 47 μC m <sup>-2</sup>	—	Sequential infiltration synthesis	177	
	1 wt% BaTiO <sub>3</sub>	Al	200 μC m <sup>-2</sup>	—	In suit polymerization, V-TENG	115	
	MoS <sub>2</sub>	PET	175 mA m <sup>-2</sup>	—	Monolayer, laminar composite	166	
	C <sub>60</sub>	AgNWs/PDMS	74.5 mA m <sup>-2</sup> , 107.2 μCm <sup>-2</sup>	—	Chemical grafting, 30N, 3Hz Corona charging, V-TENG	178	
PMMA	AlO <sub>x</sub>	PMMA	55 mA m <sup>-2</sup> , 54 μC m <sup>-2</sup>	—	Sequential infiltration synthesis	177	
BMF	1 wt% CaCu <sub>3</sub> Ti <sub>4</sub> O <sub>12</sub>	Au	25.8 mA m <sup>-2</sup>	21.74	Rotation-type TENG	169	
PEBA	0.5 vol% α-FeOOH	PET	91.1 μC m <sup>-2</sup>	—	500 N, V-TENG	127	
PA 11	Mesoporous carbon	PTFE	75 μC m <sup>-2</sup>	—	5 kV, positive charge injection	179	
PVDF		PA11	375 μC m <sup>-2</sup>	—	-7 kV, negative charge injection	—	
PVA	0.75M CaCl <sub>2</sub>	PTFE	16.875 mA m <sup>-2</sup>	—	0.4 kgf, V-TENG	191	
	H <sub>3</sub> PO <sub>4</sub>	PTFE	0.67 mA m <sup>-2</sup>	—	—	—	
TPU	10%Tp-TFAB COF	PVC	16.25 mA m <sup>-2</sup> , 94.6 μC m <sup>-2</sup>	—	40 N, 4 Hz, V-TENG	140	
	Ionic liquid	PTFE	25 mA m <sup>-2</sup> , 250 μC m <sup>-2</sup>	—	25 kPa, 4 Hz, V-TENG	192	

<sup>a</sup> V-TENG: vertical contact-separation mode TENG.

doped into PDMS (Fig. 10k), Kapton and PMMA to tune their triboelectric properties. The depth of infiltration can reach 3 μm with promising depth and stability. Not only do fillers and substrates need to be selected, doping and composite technology also need further research to obtain robust nanocomposite films.

## 5.2 Carbon-based filler composite films

Carbon-based materials such as C<sub>60</sub>,<sup>178</sup> mesoporous carbon,<sup>179</sup> active carbon,<sup>180</sup> carbon nanotubes (CNTs),<sup>181–183</sup> graphene oxide (GO) and graphene<sup>184,185</sup> are also popular fillers to enhance the triboelectric output performance of TENGs. Conductive carbon fillers have good charge stabilization and storage ability in the polymer matrix, which can improve charge density and charge-retention capacity. C<sub>60</sub> is a good electron acceptor with high electronegativity, low electron affinity and low unoccupied molecular orbitals. A chemically modified C<sub>60</sub> by an end-capping reagent is directly connected to the chain of 6FDA-APS PI to form a high performance negative polymer C<sub>60</sub>-*b*-PI (Fig. 11a).<sup>178</sup> The introduction of C<sub>60</sub> also decreases electron affinity and raises the work function value (Fig. 11c), which

determines the triboelectric property of polymers. In addition, the normalized charge density Q<sub>sc</sub> of C<sub>60</sub>-*b*-PI decays more slowly, which has a higher stable charge density compared with PI (Fig. 11b). Due to the charge accumulation and strong electron trapping ability of C<sub>60</sub>, this composite film obtains over 300 μC m<sup>-2</sup> charge density and excellent charge-retention performance. The charge trapping ability of carbon-based fillers is particularly advantageous to lock charges during high-voltage charge injection. To form charge-constrained electrostatic spinning layers, mesoporous carbon spheres (mCSs) are combined with PVDF and nylon 11, respectively.<sup>179</sup> Due to the introduction of mCSs, this layer can enhance the charge transport and charge confinement, and consequently improve the polarity and charge density (Fig. 11d). The charge-constrained layers are added under PTFE and nylon 11 as multiwall triboelectric layers, respectively. An active carbon-doped PVDF composite film is also reported for a TENG tribo-layer.<sup>180</sup> The TENG has a 9.8-fold increase in output power compared with the pure PVDF film, as a result of high relative dielectric constant and interfacial polarization caused by active carbon. As shown in Fig. 11e,

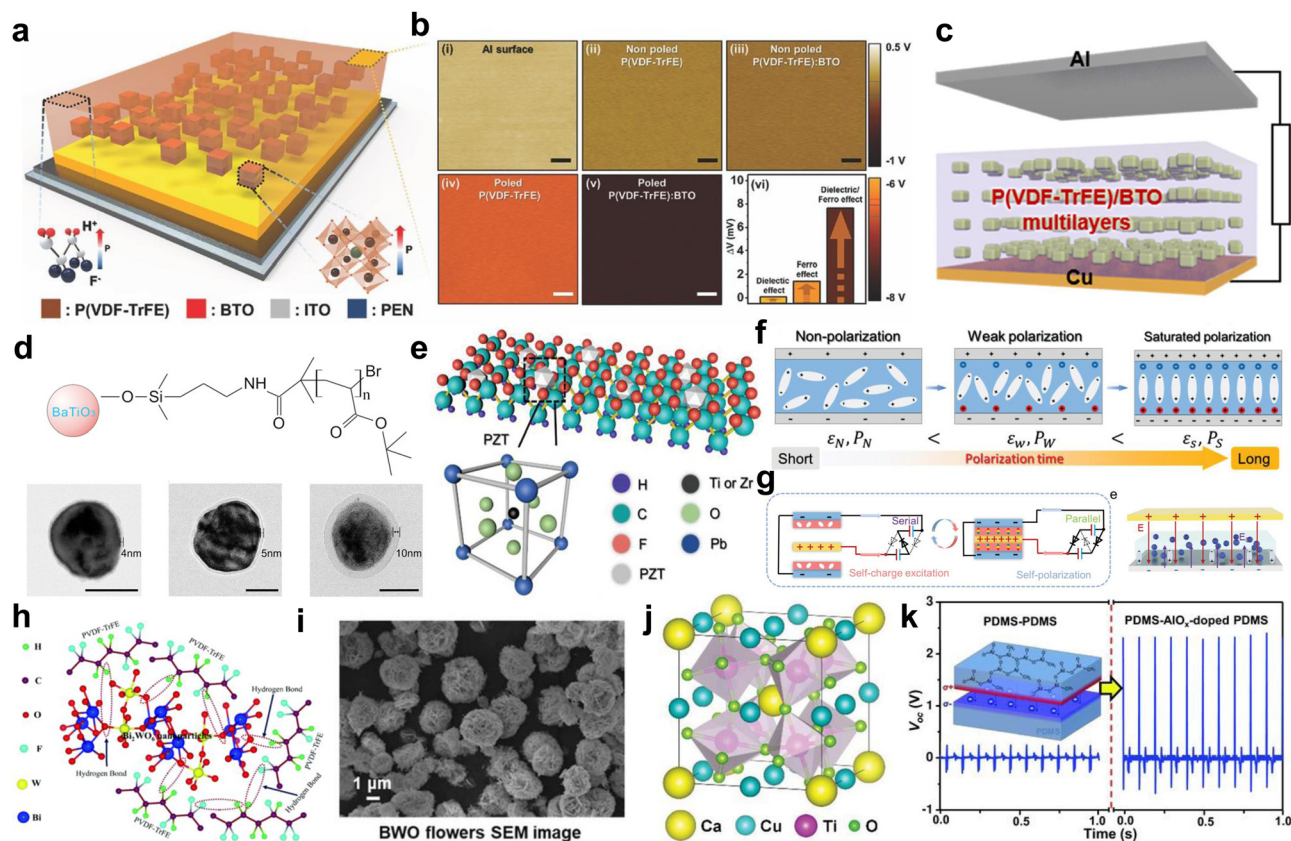


**Fig. 10** (a) Schematic description of a BaTiO<sub>3</sub>/P(VDF-TrFE)-based TENG. (b) The surface charge potential of P(VDF-TrFE) and BaTiO<sub>3</sub>/P(VDF-TrFE) composite films with/without poling, measured by KPFM. Reproduced with permission from ref. 163, Copyright 2017, WILEY-VCH. (c) Schematic of the multilayered P(VDF-TrFE)/BTO based TENG. Reproduced with permission from ref. 164, Copyright 2020, American Chemical Society. (d) Schematic diagram and TEM images of the core-shell structured BaTiO<sub>3</sub>-PtBA nanoparticles (scale bar 50 nm). Reproduced with permission from ref. 157, Copyright 2018, American Chemical Society. (e) Structure of the PZT. (f) Schematic diagram of the self-polarization process. Reproduced with permission from ref. 160, Copyright 2022, WILEY-VCH. (g) The systematic electric circuit scheme of a self-excited dielectrically polarized TENG based on the BaTiO<sub>3</sub>/PVDF film. Reproduced with permission from ref. 159, Copyright 2022, WILEY-VCH. (h) Interaction mechanism of Bi<sub>2</sub>WO<sub>6</sub> nanoparticles and the P(VDF-TrFE) polymer. Reproduced with permission from ref. 161, Copyright 2022, The Royal Society of Chemistry. (i) SEM image of the synthesized Bi<sub>2</sub>WO<sub>6</sub> marigold flower-like materials. Reproduced with permission from ref. 168, Copyright 2022, WILEY-VCH. (j) Chemical structure of CCTO. Reproduced with permission from ref. 169, Copyright 2020, WILEY-VCH. (k) The voltage of the TENG based on the PDMS-AlO<sub>x</sub>/PDMS film; the inset is a schematic of charge redistribution between pristine PDMS and AlO<sub>x</sub>-doped PDMS. Reproduced with permission from ref. 177, Copyright 2015, WILEY-VCH.

triboelectric charges accumulate around active carbon particles and have higher charge distribution by interfacial polarization.<sup>180</sup> Similar gains have been reported for carbon nanotubes,<sup>186,187</sup> graphene and graphene oxide,<sup>188–190</sup> and other carbon-based fillers for composite films to enhance the output performance of TENGs. However, the excellent electrical conductivity of the carbon material limits the filler content and enhancement of triboelectric properties. Excessive carbon-based fillers will reduce dielectric properties, resulting in dielectric breakdown, loss of charge retention and limitation ability. The performance and parameters of inorganic/organic composite films are summarized in Table 2.

### 5.3 Ion and electrolyte composite films

Doping conductive ions and electrolyte fillers with charge transport and migration ability can also promote the triboelectric properties of ionic polymers. The solid polymer electrolytes (SPE) consisting of electrolytes with asymmetric ion pairing, such as

HCl, CaCl<sub>2</sub> and H<sub>3</sub>PO<sub>4</sub>, and PVA matrix have been reported.<sup>191</sup> When CaCl<sub>2</sub> with more anions was added in PVA, the surface potential decreased after contact (Fig. 11f) and high-energy electron charged states were created, according to more positive triboelectric polarity compared with pure PVA. When H<sub>3</sub>PO<sub>4</sub> with more cations was added, the surface potential increased after contact (Fig. 11f) and low-energy electron unoccupied states were created, according to more negative triboelectric polarity compared with pure PVA. By varying the type and concentration of ionic electrolyte, the electron charged states and polarity of PVA can be adjusted. A viscoelastic thermoplastic polyurethane (TPU) based polymer ion pump containing ionic liquid is also reported to fabricate a transparent and deformable TENG (Fig. 11g).<sup>192</sup> The electrical double layer (EDL) can be formed on the surface due to ion migration in the ionic liquid to enhance charge density. Moreover, hydrogels and ionic gels having a large number of mobile ions are also reported as promising stretchable triboelectric polymers, which can be applied in electronic

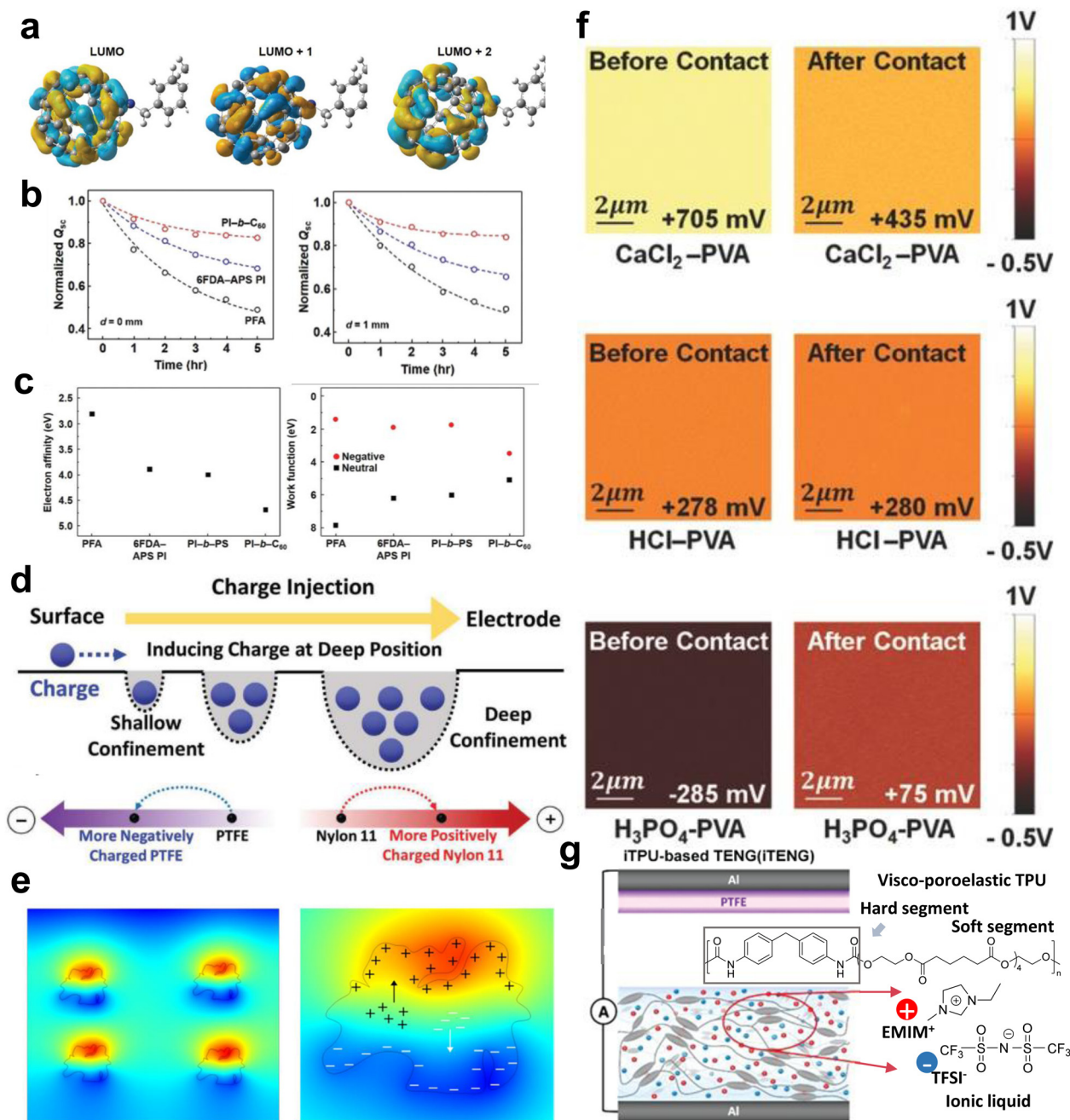


Fig. 11 (a) The molecular orbital visualization of PI-*b*-C<sub>60</sub>. (b) The normalized charge densities measured in contact mode and non-contact mode TENGs fabricated with PFA, 6FDA-APS PI, and PI-*b*-C<sub>60</sub> films. (c) The EA value and work function of PI-*b*-C<sub>60</sub>, compared with other PIs and PFA. Reproduced with permission from ref. 178, Copyright 2021, The Royal Society of Chemistry. (d) Charge transport and confinement mechanism in the mCS composite film during the charge-injection process, and resulting ranking shift of PTFE and Nylon 11. Reproduced with permission from ref. 179, Copyright 2022, Wiley-VCH. (e) Corresponding simulation of the electric field and charge distribution around AC particles by COMSOL Multiphysics. Reproduced with permission from ref. 180, Copyright 2020, American Chemical Society. (f) The surface potential of 0.75 M CaCl<sub>2</sub>-PVA SPE, 1 M HCl-PVA SPE, and 1.5 M H<sub>3</sub>PO<sub>4</sub>-PVA SPE before and after contact electrification with pristine PVA. Reproduced with permission from ref. 191, Copyright 2017, WILEY-VCH. (g) Visco-poroelastic ion pumping polymer matrix realized by embedding ionic liquids in a TPU matrix. Reproduced with permission from ref. 192, Copyright 2019, WILEY-VCH.

skin/tattoo, self-powered sensors and flexible devices.<sup>193–198</sup> Ion-doped flexible polymers can also be used as stretchable electrodes to improve the output performance of TENGs by forming an EDL effect.<sup>199,200</sup> Gel or ion polymer composites with ionic materials have great potential for flexible, stretchable TENG applications.

## 6. Triboelectric polymer handbook

In order to enlighten the understanding of the properties of triboelectric polymers and guide their design and synthesis, a triboelectric polymer handbook is summarized in Table 3. This handbook can also provide guidance on triboelectric polymer



Table 3 A list of the functional groups, representative polymers and triboelectric performance in TENG application

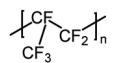
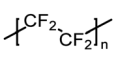
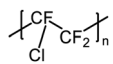
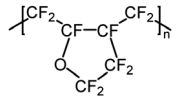
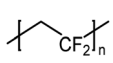
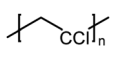
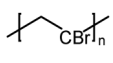
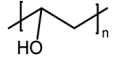
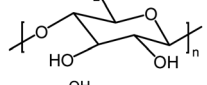
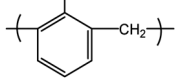
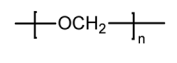
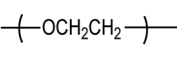
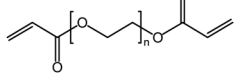
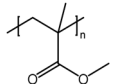
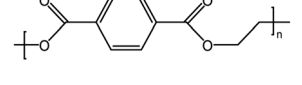
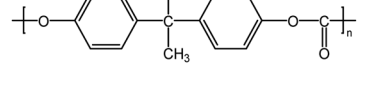
Functional groups	Representative polymer	Abbr.	Triboelectric property		Other advantages and functional prospects for TENG	Development strategy
			$\sigma$ ( $\mu\text{C m}^{-2}$ )	Polarity		
-F		FEP	352(-) <sup>15</sup>	Very negative	Hydrophobic, transparent, good thermal properties, and better processability than PTFE	Copolymerization with other vinyl monomers such as ethylene, vinylidene fluoride, sulfonyl fluoride vinyl ether, 2,2,4-trifluoro-5-trifluoromethoxy-1,3-dioxole, perfluoro-2,2-dimethyldioxole, etc. Improver processability
		PTFE	113.06(-)	Very negative	Chemical resistance, low coefficient of friction, low dielectric constant, hydrophobic, high melting	
		PCTFE	—	Very negative	Hydrophobic, chemical resistance, good air tightness and low water absorption	
		Cytop <sup>®</sup>	—	Very negative	High optical transparency, high processability, hydrophobic <sup>223-225</sup>	
		PVDF	87.35(-)	Quite negative	Good toughness, has abundant moments, has piezoelectric, ferroelectric, dielectric properties	
-Cl		PVC	117.53(-)	Very negative	Low cost, vacuum triboelectric charge density <sup>84</sup>	Plastification and modification
-Br		Poly(vinyl bromide)	0.14(-) <sup>96b</sup>	Slight negative	Flame retardant and thermal stability <sup>226-228</sup>	Mature preparation and synthesis methods, conformational control
-OH		PVA	48.6(+) <sup>140</sup>	Slight negative	Water-soluble, hydrophilia	Prepare hydrogel and ion gel
		Cellulose	0.14 W m <sup>-2</sup> , <sup>229</sup>	Slight positive	Unique optical and mechanical properties, low-cost, eco-friendly <sup>122</sup>	Chemical modification, reconstruction,
		Phenolic resin	—	Slight positive	Flame retardant and thermal stability, transparency	Composite with fiber or filler, design and change monomers
-O-		POM	344.2 <sup>230</sup>	Quite positive	Wear-resisting, good thermal stability, excellent comprehensive performance	Copolymerization, composite with fiber or filler
		PEO	154(+) <sup>123</sup>	Quite positive	Good processability, bio-compatible, water-soluble, and low-cost	Composite with fiber or filler, self-assembly <sup>122</sup>
		PEGDA	4(+) <sup>141</sup>	Quite positive	Water-soluble, can be used to prepare hydrogels	Molecular structure design and copolymerization
		PMMA	48.73(-)	Slight negative	Excellent transparency, low cost and available,	Blending, copolymerization
R'-O-C(=O)-R		PET	89.44(-)	Slight negative	Transparency, low cost and available,	Design monomers, composite with inorganic fillers
		PC	104.63(-)	Slight negative	High optical transparency, a kind of engineering plastic with excellent comprehensive properties	Glass fiber reinforcement

Table 3 (continued)

Functional groups	Representative polymer	Abbr.	Triboelectric property $\sigma$ ( $\mu\text{C m}^{-2}$ )	Polarity	Other advantages and functional prospects for TENG	Development strategy
		Kapton (PMDA-ODA PI)	92.88(-)	Quite negative	High $T_g$ , heat resistance, excellent mechanical properties and electrical insulation property	Monomer design and selection, copolymerization with polyester, polyamide, polysulfone, polyether, etc. Composite with inorganic fillers to enhance mechanical characteristics, or composite with rubber to improve impact resistance
		PA6	18.35(-)	Very positive	Similar with PA66, better impact resistance and solubility resistance	
		PA66	26.09(-)	Very positive	Strong strength and stiffness, hygroscopicity, high $T_g$ (260–290 °C)	
		PA11	74 mA $\text{m}^{-2}(+)^{153}$	Quite positive	Low water absorption, good oil resistance, low temperature resistance, easy processing	Blending or composite with inorganic fillers
		IU	42.11 mA $\text{m}^{-2}(+)^{119}$	Very positive	Anticorrosive, water-proof, wear-resistant	Design monomers, composite with inorganic fillers and fibers, development of process technology
		PU	30 mA $\text{m}^{-2, 217}$	Slight positive	Low cost and available, rich products, elasticity and stretchability	Design chemical structure to achieve functional advantages such as super stretchability, self-healing
		BMF	24 mA $\text{m}^{-2}(+)^{117}$	Very positive	High mechanical durability, hard	Design and synthesize monomers, composite with inorganic fillers
$-\text{C}\equiv\text{N}$		PAN	$\sim 250(+)^{231}$	Quite positive	Good weather resistance and durability as fiber	Copolymerization modification
$-\text{NH}-$		PAn	0.04(-) <sup>96</sup>	Slight positive	Electrical conductivity and electrochemical properties after doping	Doping technology and its application
$-\text{NH}_2$		Polyallylamine	0.18(+) <sup>96</sup>	Very positive	Biocompatibility, adhesion <sup>232,233</sup>	Study on synthesis technology and properties
		PSF	18.92(-)	Slight positive	Wear resistance, self-extinguishing property, high thermal stability, excellent mechanical properties, high dielectric strength	Design and synthesize monomers, copolymerization with PI, PEEK, etc. glass fiber reinforcement
		Fluorinated poly(S-r-DIB)	0.4 mA $\text{m}^{-2}(-)^{99}$	Very negative	High electron affinity, low-cost, eco-friendly	Mature, safe and non-toxic synthesis and production methods, blending
$-\text{S}-$		PPS	31.82(-)	Slight negative	Excellent high temperature resistance, corrosion resistance, radiation resistance, flame retardant, dimensional stability and excellent electrical properties	Chemical modification to enhance toughness and mechanical strength, fabricate composite materials as fiber
		PDMS	102.05(-)	Quite negative	Flexible, super stretchable, transparency, viscosity	Design and application of structure and performance

Table 3 (continued)

Functional groups	Representative polymer	Abbr.	Triboelectric property		Other advantages and functional prospects for TENG	Development strategy
			$\sigma$ ( $\mu\text{C m}^{-2}$ )	Polarity		
-CH <sub>3</sub>		PE	71.20(-)	Neutral	Low cost, have been mass-produced, non-polar electret	Copolymerization, composite film, electret and processing technology
		PP	27.23(-)	Neutral		
		Unsaturated PTFE	13.75(-) <sup>83</sup>	Very negative	Prepared by sputtering, C-F bond with sp <sup>2</sup> hybridization, strong electron absorption ability	Mature preparation and synthesis methods
		PS	103.48(-)	Slight positive	High transparency, excellent insulation but brittle	Copolymerization to prepare HIPS, improve triboelectric property
		Poly(4-vinylpyridine)	0.51(+) <sup>96</sup>	Quite negative	Electrical conductivity and electrochemical properties	Study on synthesis technology and properties

<sup>a</sup> The data, without related reference, are derived from the absolute value of charge density in the triboelectric series by contacting with mercury.<sup>82</sup>

<sup>b</sup> The data are obtained from ref. 96 by using PVA as another tribo-layer.

selection for TENG researchers. For excellent negative triboelectric polymers, PTFE is usually the most popular candidate because of its advantages of high charge density, low coefficient of friction, and low dielectric constant. Moreover, rich PTFE copolymers can be obtained through copolymerization with other olefin monomers such as PFSA, PFA, FEP, ETFE, Hyflon<sup>®</sup> AD, and Teflon<sup>®</sup> AF. The introduction of different monomers can improve the processability and obtain other functional advantages such as transparency and processability, while retaining excellent triboelectric performance. Positive polymers are usually nitrogen-containing condensation polymers such as nylon and amino resin, which also have a lot of monomers and designability. The design, synthesis and selection of monomers is an effective means to change the triboelectric properties of polymers. Moreover, adding or changing the process technology can also change the aggregate structure and crystallinity, which is closely related to triboelectric properties. In Table 3, the representative polymers and their reported triboelectric properties are summarized, and the triboelectric polarity of a polymer is determined by its ranking or predicted ranking in the triboelectric series.<sup>82,88</sup> For high output performance and energy conversion efficiency of TENGs, the polymer at either end of the triboelectric series is the preferred choice. Potential development strategies to enhance the triboelectric capacity of polymers are also listed in Table 3.

For the diverse applications and requirements of TENGs, functional advantages also influence the choice of triboelectric polymers. Endowing triboelectric materials with functional application without sacrificing triboelectric properties is of great significance for practical application. For example, fluoropolymer films such as PFA and FEP are ideal tribo-layers for solid-liquid TENGs and combining with solar energy, due to their excellent hydrophobicity and transmittance.<sup>206–208</sup> High glass transition temperature ( $T_g$ ) and thermal stability are required properties for application in high temperature conditions and self-powered

fire alarm systems.<sup>209,210</sup> Meanwhile, low cost, good processability triboelectric materials are also needed for large-scale production and applications of TENGs.<sup>211–213</sup> The wear-resistant, durable triboelectric polymer is conducive to the long-term stable operation of the contact mode TENG, while charge-stable triboelectric polymers are beneficial to the performance of contactless TENGs. In addition, advanced triboelectric polymers with biocompatible,<sup>214–216</sup> self-healing,<sup>217,218</sup> ultra-stretchable,<sup>219–221</sup> stimuli-responsive,<sup>222</sup> and other properties are relevant to TENG application in biomedical, wearable electronic devices, intelligent sensors, and extreme environments. The functional properties of common triboelectric polymers are summarized in Table 3.

## 7. Summary and perspectives

Recent progress in the study of triboelectric polymers and related synthesis strategies are summarized in this review. The functional groups and their density in the chemical structure lead to different HOMO energy levels, which is the key element for regulating the electrification of both negative/positive triboelectric polymers. According to the previous studies, rich halogens with strong electron-withdrawing or amino groups with electron-donating ability in monomers are usually chosen for fabricating triboelectric polymers, due to their strong polarities. A series of functional groups and their representative polymers with different triboelectric properties and functional advantages are listed in Table 3. For negative polymers, the groups such as fluorine, chlorine, imide, siloxane and their derivatives can be designed and modified, while amide, urea, nitrile group, amino resin, *etc.* are promising for fabricating positive polymers. On the other hand, the energy level structure with a large HOMO-LUMO gap can give more localized states for electron transfer, which usually leads to high charge density during contact electrification. Accordingly, this review discusses several different approaches for

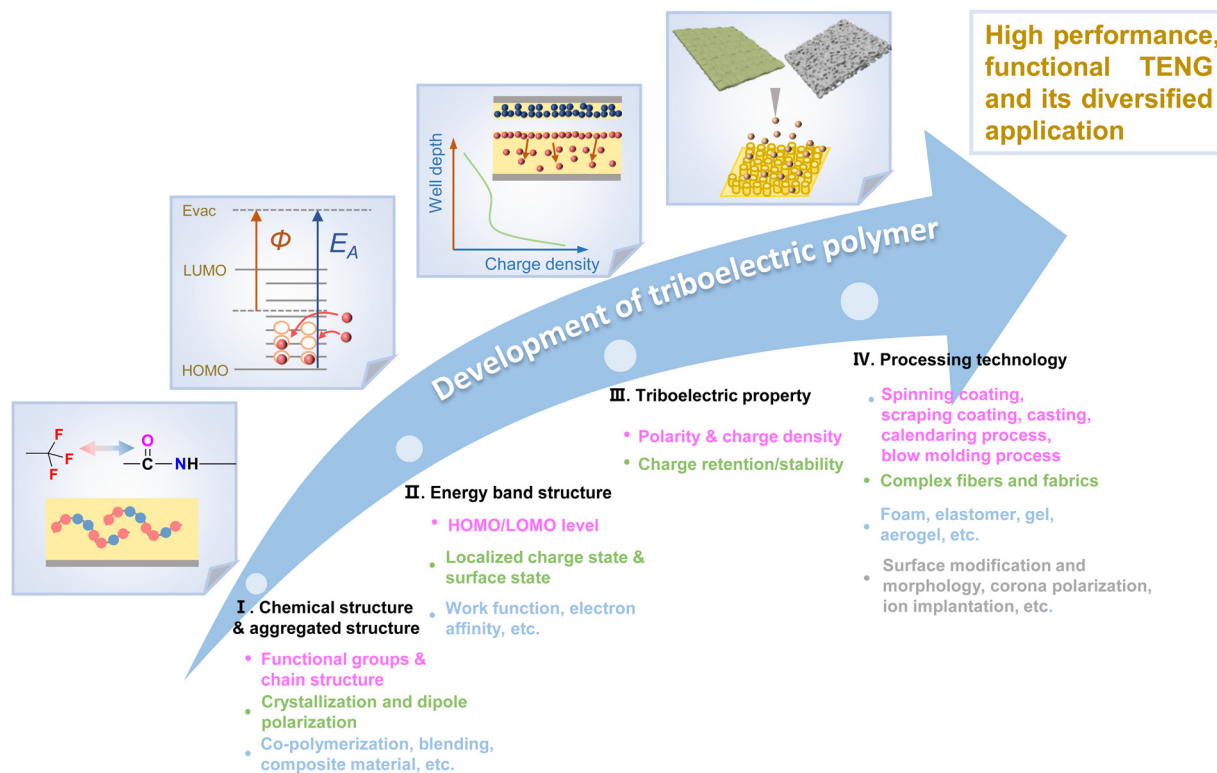


Fig. 12 Schematic diagram of the development of triboelectric polymers.

tuning the energy level structure of triboelectric polymers. Co-polymerization, blending and annealing processes, which can increase crystallization, heterogeneous interfaces and dipole orientation, also generates a wide gap and improves the capability of contact electrification. In addition, doping with high dielectric constant inorganic fillers, and carbon-based fillers for charge storage or transferable electrolytes as listed in Table 2 is also an effective approach to modify localized charge states, interfacial polarization and deep traps for triboelectric polymers. With the development of TENGs, more and more polymers have been designed and synthesized, while their applications in many areas have been attempted. This review can be of great help to the research on triboelectric polymers for the practical studies and innovations of diversified TENGs, as well as facilitating applications in many fields related to the polymer materials.

The large-scale preparation and extensive application of the triboelectric polymer with high charge density, strong polarity and excellent charge stability are required for high performance TENGs. As shown in Fig. 12, further improvements of triboelectric polymers can be achieved by resolving the following challenges.

(1) More polymers with strong electrification polarity, high charge density and excellent charge stability are required for high performance TENGs, which play an important role in improving the output and energy conversion efficiency of TENGs.

(2) The strong, wear-resistant composite materials and copolymers still need further research to regulate and increase triboelectric properties. What's more, the principle and mechanism based on those approaches can be further systematically and comprehensively understood.

(3) The relationship between the chemical structure and triboelectric property of polymers is still vague without a unified and comprehensive understanding. This relationship can guide the synthesis and selection of triboelectric polymers and also shed light on the physical mechanism of contact electrification.

(4) The study of synthesis and preparation methods suitable for large-scale and low-cost synthesis provides the basis for the extensive and large-scale applications of TENGs. It is also necessary to endow polymers with functional characteristics without sacrificing triboelectric properties, which can satisfy the diversified applications of TENGs in various environments.

(5) The post-processing technology of polymers results in a variety of triboelectric forms, which are suitable for the practical application environment. The advantages of triboelectric polymers can be further enhanced through post-treatment, and the performance and function of TENGs can be maximized.

## Conflicts of interest

The authors declare no conflict of interests.

## Acknowledgements

This work was supported by the National Key R&D Project from Minister of Science and Technology (2021YFA1201601), National Natural Science Foundation of China (Grant No. 62174014 and 52322313), Beijing Nova program (Z201100006820063), Youth Innovation Promotion Association CAS (2021165), Innovation

Project of Ocean Science and Technology (22-3-3-hygg-18-hy), State Key Laboratory of New Ceramic and Fine Processing Tsinghua University (KFZD202202), Fundamental Research Funds for the Central Universities (292022000337), Young Top-Notch Talents Program of Beijing Excellent Talents Funding (2017000021223ZK03).

## References

- 1 S. Wang, L. Lin and Z. L. Wang, *Nano Lett.*, 2012, **12**, 6339–6346.
- 2 F. R. Fan, L. Lin, G. Zhu, W. Wu, R. Zhang and Z. L. Wang, *Nano Lett.*, 2012, **12**, 3109–3114.
- 3 C. S. Wu, A. C. Wang, W. B. Ding, H. Y. Guo and Z. L. Wang, *Adv. Energy Mater.*, 2019, **9**, 1802906.
- 4 W. Xu, H. Zheng, Y. Liu, X. Zhou, C. Zhang, Y. Song, X. Deng, M. Leung, Z. Yang, R. X. Xu, Z. L. Wang, X. C. Zeng and Z. Wang, *Nature*, 2020, **578**, 392–396.
- 5 R. Hinchet, H. J. Yoon, H. Ryu, M. K. Kim, E. K. Choi, D. S. Kim and S. W. Kim, *Science*, 2019, **365**, 491–494.
- 6 Y. Zi, J. Wang, S. Wang, S. Li, Z. Wen, H. Guo and Z. L. Wang, *Nat. Commun.*, 2016, **7**, 10987.
- 7 J. Tian, X. Chen and Z. L. Wang, *Nanotechnology*, 2020, **31**, 242001.
- 8 Z. L. Wang, *ACS Nano*, 2013, **7**, 9533–9557.
- 9 Y. Shi, F. Wang, J. Tian, S. Li, E. Fu, J. Nie, R. Lei, Y. Ding, X. Chen and Z. L. Wang, *Sci. Adv.*, 2021, **7**, eabe2943.
- 10 G. L. Liu, H. Y. Guo, S. X. Xu, C. G. Hu and Z. L. Wang, *Adv. Energy Mater.*, 2019, **9**, 1900801.
- 11 C. G. Zhang, L. X. He, L. L. Zhou, O. Yang, W. Yuan, X. L. Wei, Y. B. Liu, L. Lu, J. Wang and Z. L. Wang, *Joule*, 2021, **5**, 1613–1623.
- 12 R. Lei, Y. X. Shi, Y. F. Ding, J. H. Nie, S. Y. Li, F. Wang, H. Zhai, X. Y. Chen and Z. L. Wang, *Energy Environ. Sci.*, 2020, **13**, 2178–2190.
- 13 X. Y. Li, C. G. Zhang, Y. K. Gao, Z. H. Zhao, Y. X. Hu, O. Yang, L. Liu, L. L. Zhou, J. Wang and Z. L. Wang, *Energy Environ. Sci.*, 2022, **15**, 1334–1345.
- 14 S. Y. Li, Y. Fan, H. Q. Chen, J. H. Nie, Y. X. Liang, X. L. Tao, J. Zhang, X. Y. Chen, E. G. Fu and Z. L. Wang, *Energy Environ. Sci.*, 2020, **13**, 896–907.
- 15 Z. Liu, Y. Huang, Y. Shi, X. Tao, H. He, F. Chen, Z. X. Huang, Z. L. Wang, X. Chen and J. P. Qu, *Nat. Commun.*, 2022, **13**, 4083.
- 16 Z. Zhao, Y. Dai, D. Liu, L. Zhou, S. Li, Z. L. Wang and J. Wang, *Nat. Commun.*, 2020, **11**, 6186.
- 17 D. Liu, X. Yin, H. Guo, L. Zhou, X. Li, C. Zhang, J. Wang and Z. L. Wang, *Sci. Adv.*, 2019, **5**, eaav6437.
- 18 F. Wang, J. Tian, Y. Ding, Y. Shi, X. Tao, X. Wang, Y. Yang, X. Chen and Z. L. Wang, *iScience*, 2021, **24**, 102502.
- 19 Z. Wang, W. L. Liu, W. C. He, H. Y. Guo, L. Long, Y. Xi, X. Wang, A. P. Liu and C. G. Hu, *Joule*, 2021, **5**, 441–455.
- 20 J. Chen and Z. L. Wang, *Joule*, 2017, **1**, 480–521.
- 21 G. Khandelwal, N. P. M. J. Raj and S. J. Kim, *Adv. Energy Mater.*, 2021, **11**, 2101170.
- 22 Y. S. Choi, S. W. Kim and S. Kar-Narayan, *Adv. Energy Mater.*, 2021, **11**, 2003802.
- 23 A. Chen, C. Zhang, G. Zhu and Z. L. Wang, *Adv. Sci.*, 2020, **7**, 2000186.
- 24 Z. L. Wang, *Nano Energy*, 2020, **68**, 104272.
- 25 H. Staudinger, *Ber. Dtsch. Chem. Ges.*, 1920, **53**, 1073–1085.
- 26 M. S. Silverstein, *Polymer*, 2021, **215**, 123409.
- 27 C. K. Varnava and C. S. Patrickios, *Polymer*, 2021, **215**, 123322.
- 28 A. S. Abd-El-Aziz, M. Antonietti, C. Barner-Kowollik, W. H. Binder, A. Boker, C. Boyer, M. R. Buchmeiser, S. Z. D. Cheng, F. D'Agosto, G. Floudas, H. Frey, G. Galli, J. Genzer, L. Hartmann, R. Hoogenboom, T. Ishizone, D. L. Kaplan, M. Leclerc, A. Lendlein, B. Liu, T. E. Long, S. Ludwigs, J. F. Lutz, K. Matyjaszewski, M. A. R. Meier, K. Mullen, M. Mullner, B. Rieger, T. P. Russell, D. A. Savin, A. D. Schluter, U. S. Schubert, S. Seiffert, K. Severing, J. B. P. Soares, M. Staffilani, B. S. Sumerlin, Y. M. Sun, B. Z. Tang, C. B. Tang, P. Theato, N. Tirelli, O. K. C. Tsui, M. M. Unterlass, P. Vana, B. Voit, S. Vyazovkin, C. Weder, U. Wiesner, W. Y. Wong, C. Wu, Y. Yagci, J. Y. Yuan and G. Z. Zhang, *Macromol. Chem. Phys.*, 2020, **221**, 2000216.
- 29 J. Lopez, D. G. Mackanic, Y. Cui and Z. N. Bao, *Nat. Rev. Mater.*, 2019, **4**, 312–330.
- 30 X. Chen, L. Qiu, J. Ren, G. Guan, H. Lin, Z. Zhang, P. Chen, Y. Wang and H. Peng, *Adv. Mater.*, 2013, **25**, 6468.
- 31 H. K. Song and G. T. R. Palmore, *Adv. Mater.*, 2006, **18**, 1764–1768.
- 32 K. Song, D. A. Agyeman, M. Park, J. Yang and Y. M. Kang, *Adv. Mater.*, 2017, **29**, 1606572.
- 33 Y. Yusran, Q. Fang and V. Valtchev, *Adv. Mater.*, 2020, **32**, 2002038.
- 34 M. Zhang, B. Li, J. J. Wang, H. B. Huang, L. Zhang and L. Q. Chen, *Adv. Mater.*, 2021, **33**, 2008198.
- 35 S. Y. Lee, C. H. Park, J. E. Chae, S. Lee, H. J. Lee, S. J. Yoo, J. Y. Kim, J. H. Jang and H. J. Kim, *Adv. Eng. Mater.*, 2021, **23**, 2001174.
- 36 S. Yuk, M. J. Choo, D. Lee, H. Guim, T. H. Kim, D. G. Lee, S. Choi, D. H. Lee, G. Doo, Y. T. Hong and H. T. Kim, *Adv. Mater.*, 2017, **29**, 1603056.
- 37 Y. Yan, X. Liu and T. Wang, *Adv. Mater.*, 2017, **29**, 1601674.
- 38 L. Ma, Y. Cui, J. Zhang, K. Xian, Z. Chen, K. Zhou, T. Zhang, W. Wang, H. Yao, S. Zhang, X. Hao, L. Ye and J. Hou, *Adv. Mater.*, 2023, **35**, 2208926.
- 39 D. Meng, R. Zheng, Y. Zhao, E. Zhang, L. Dou and Y. Yang, *Adv. Mater.*, 2022, **34**, 2107330.
- 40 P. C. Mondal, N. Kantor-Uriel, S. P. Mathew, F. Tassinari, C. Fontanesi and R. Naaman, *Adv. Mater.*, 2015, **27**, 1924–1927.
- 41 R. Schroot, M. Jager and U. S. Schubert, *Chem. Soc. Rev.*, 2017, **46**, 2754–2798.
- 42 X. Chen, Y. Wu, J. Shao, T. Jiang, A. Yu, L. Xu and Z. L. Wang, *Small*, 2017, **13**, 1702929.
- 43 Y. C. Lai, J. Deng, S. Niu, W. Peng, C. Wu, R. Liu, Z. Wen and Z. L. Wang, *Adv. Mater.*, 2016, **28**, 10024–10032.
- 44 S. Shu, Z. Wang, P. Chen, J. Zhong, W. Tang and Z. L. Wang, *Adv. Mater.*, 2023, **35**, 2211385.
- 45 G. Khandelwal and R. Dahiya, *Adv. Mater.*, 2022, **34**, 2200724.

- 46 X. Pu, C. Zhang and Z. L. Wang, *Natl. Sci. Rev.*, 2023, **10**, nwac170.
- 47 Y. Yang, X. Guo, M. Zhu, Z. Sun, Z. Zhang, T. He and C. Lee, *Adv. Energy Mater.*, 2022, **13**, 2203040.
- 48 D. Zhang, D. Wang, Z. Xu, X. Zhang, Y. Yang, J. Guo, B. Zhang and W. Zhao, *Coord. Chem. Rev.*, 2021, **427**, 213597.
- 49 Q. Zhou, J. Pan, S. Deng, F. Xia and T. Kim, *Adv. Mater.*, 2021, **33**, 2008276.
- 50 F. Invernizzi, S. Dulio, M. Patrini, G. Guizzetti and P. Mustarelli, *Chem. Soc. Rev.*, 2016, **45**, 5455–5473.
- 51 C. Rodrigues, D. Nunes, D. Clemente, N. Mathias, J. M. Correia, P. Rosa-Santos, F. Taveira-Pinto, T. Morais, A. Pereira and J. Ventura, *Energy Environ. Sci.*, 2020, **13**, 2657–2683.
- 52 Q. Zhang, C. F. Xin, F. Shen, Y. Gong, Y. L. Zi, H. Y. Guo, Z. J. Li, Y. Peng, Q. Zhang and Z. L. Wang, *Energy Environ. Sci.*, 2022, **15**, 3688–3721.
- 53 Z. L. Wang, *Faraday Discuss.*, 2014, **176**, 447–458.
- 54 C. Wu, A. C. Wang, W. Ding, H. Guo and Z. L. Wang, *Adv. Energy Mater.*, 2019, **9**, 1802906.
- 55 Z. L. Wang, J. Chen and L. Lin, *Energy Environ. Sci.*, 2015, **8**, 2250–2282.
- 56 S. M. Niu, S. H. Wang, L. Lin, Y. Liu, Y. S. Zhou, Y. F. Hu and Z. L. Wang, *Energy Environ. Sci.*, 2013, **6**, 3576–3583.
- 57 H. Zou, L. Guo, H. Xue, Y. Zhang, X. Shen, X. Liu, P. Wang, X. He, G. Dai, P. Jiang, H. Zheng, B. Zhang, C. Xu and Z. L. Wang, *Nat. Commun.*, 2020, **11**, 2093.
- 58 S. Niu, S. Wang, Y. Liu, Y. S. Zhou, L. Lin, Y. Hu, K. C. Pradel and Z. L. Wang, *Energy Environ. Sci.*, 2014, **7**, 2339–2349.
- 59 Y. Zi, S. Niu, J. Wang, Z. Wen, W. Tang and Z. L. Wang, *Nat. Commun.*, 2015, **6**, 8376.
- 60 J. Wang, C. Wu, Y. Dai, Z. Zhao, A. Wang, T. Zhang and Z. L. Wang, *Nat. Commun.*, 2017, **8**, 88.
- 61 E. Fukada and J. F. Fowler, *Nature*, 1958, **181**, 693–694.
- 62 R. C. Plumb and W. T. Scott, *J. Chem. Educ.*, 1971, **48**, 524.
- 63 W. R. Harper, *Proc. R. Soc. London, Ser. A*, 1951, **205**, 83–103.
- 64 Z. W. Ren, J. H. Nie, J. J. Shao, Q. S. Lai, L. F. Wang, J. Chen, X. Y. Chen and Z. L. Wang, *Adv. Funct. Mater.*, 2018, **28**, 1802989.
- 65 Y. Wang, H. Wu, L. Xu, H. Zhang, Y. Yang and Z. L. Wang, *Sci. Adv.*, 2020, **6**, eabb9083.
- 66 S. Lin, L. Xu, C. Xu, X. Chen, A. C. Wang, B. Zhang, P. Lin, Y. Yang, H. Zhao and Z. L. Wang, *Adv. Mater.*, 2019, **31**, 1808197.
- 67 B. Cheng, Q. Xu, Y. Ding, S. Bai, X. Jia, Y. Yu, J. Wen and Y. Qin, *Nat. Commun.*, 2021, **12**, 4782.
- 68 X. K. Yu, S. K. Fu, X. L. Zuo, J. Zeng, C. C. Shan, W. C. He, W. P. Li and C. G. Hu, *Adv. Funct. Mater.*, 2022, **32**, 2207498.
- 69 O. Verners, L. Lapčinskis, L. Ģermane, A. Kasikov, M. Timusk, K. Pudzs, A. V. Ellis, P. C. Sherrell and A. Šutka, *Nano Energy*, 2022, **104**, 107914.
- 70 A. Sutka, K. Malnieks, L. Lapcinskis, M. Timusk, K. Kalnins, A. Kovalovs, J. Biteniekis, M. Knite, D. Stevens and J. Grunlan, *Phys. Chem. Chem. Phys.*, 2020, **22**, 13299–13305.
- 71 G. S. P. Castle, *IEEE Ind. Appl. Mag.*, 2010, **16**, 8–13.
- 72 K. Ohara, *J. Electrostat.*, 1986, **18**, 179–192.
- 73 H. T. Baytekin, A. Z. Patashinski, M. Branicki, B. Baytekin, S. Soh and B. A. Grzybowski, *Science*, 2011, **333**, 308–312.
- 74 F. Galembeck, T. A. L. Burgo, L. B. S. Balestrin, R. F. Gouveia, C. A. Silva and A. Galembeck, *RSC Adv.*, 2014, **4**, 64280–64298.
- 75 C. Y. Liu and A. J. Bard, *J. Am. Chem. Soc.*, 2009, **131**, 6397–6401.
- 76 C. Liu and A. J. Bard, *Nat. Mater.*, 2008, **7**, 505–509.
- 77 J. Zhang, M. L. Coote and S. Ciampi, *J. Am. Chem. Soc.*, 2021, **143**, 3019–3032.
- 78 M. W. Williams, *AIP Adv.*, 2012, **2**, 010701.
- 79 D. J. Lacks and T. Shinbrot, *Nat. Rev. Chem.*, 2019, **3**, 465–476.
- 80 J. Henniker, *Nature*, 1962, **196**, 474.
- 81 A. F. Diaz and R. M. Felix-Navarro, *J. Electrostat.*, 2004, **62**, 277–290.
- 82 H. Zou, Y. Zhang, L. Guo, P. Wang, X. He, G. Dai, H. Zheng, C. Chen, A. C. Wang, C. Xu and Z. L. Wang, *Nat. Commun.*, 2019, **10**, 1427.
- 83 S. Li, J. Nie, Y. Shi, X. Tao, F. Wang, J. Tian, S. Lin, X. Chen and Z. L. Wang, *Adv. Mater.*, 2020, **32**, 2001307.
- 84 D. Liu, L. Zhou, S. Cui, Y. Gao, S. Li, Z. Zhao, Z. Yi, H. Zou, Y. Fan, J. Wang and Z. L. Wang, *Nat. Commun.*, 2022, **13**, 6019.
- 85 S. H. Shin, Y. H. Kwon, Y. H. Kim, J. Y. Jung, M. H. Lee and J. Nah, *ACS Nano*, 2015, **9**, 4621–4627.
- 86 S. H. Shin, Y. E. Bae, H. K. Moon, J. Kim, S. H. Choi, Y. Kim, H. J. Yoon, M. H. Lee and J. Nah, *ACS Nano*, 2017, **11**, 6131–6138.
- 87 H. Y. Li, L. Su, S. Y. Kuang, C. F. Pan, G. Zhu and Z. L. Wang, *Adv. Funct. Mater.*, 2015, **25**, 5691–5697.
- 88 Y. Liu, J. Mo, Q. Fu, Y. Lu, N. Zhang, S. Wang and S. Nie, *Adv. Funct. Mater.*, 2020, **30**, 2004714.
- 89 D. K. Davies, *J. Phys. D: Appl. Phys.*, 1969, **2**, 1533–1537.
- 90 Y. Zhang, Z. Zhou, L. Sun, Z. Liu, X. Xia and T. H. Tao, *Adv. Mater.*, 2018, **30**, 1805722.
- 91 D. Kang, H. Y. Lee, J.-H. Hwang, S. Jeon, D. Kim, S. Kim and S.-W. Kim, *Nano Energy*, 2022, **100**, 107531.
- 92 L. Z. Li, X. L. Wang, P. Z. Zhu, H. Q. Li, F. Wang and J. Wu, *Nano Energy*, 2020, **70**, 104476.
- 93 H. W. Gibson and F. C. Bailey, *Chem. Phys. Lett.*, 1977, **51**, 352–355.
- 94 I. Shinohara, F. Yamamoto, H. Anzai and S. Endo, *J. Electrostat.*, 1976, **2**, 99–110.
- 95 H. Ko, Y. W. Lim, S. Han, C. K. Jeong and S. B. Cho, *ACS Energy Lett.*, 2021, **6**, 2792–2799.
- 96 X. Zhang, L. F. Chen, Y. Jiang, W. C. Lim and S. Soh, *Chem. Mater.*, 2019, **31**, 1473–1478.
- 97 A. Šutka, K. Mālnieks, L. Lapčinskis, P. Kaufelde, A. Linarts, A. Bērziņa, R. Zābels, V. Jurkāns, I. Gorņevs, J. Blūms and M. Knite, *Energy Environ. Sci.*, 2019, **12**, 2417–2421.

- 98 L. Lapčinskis, K. Mālnieks, J. Blūms, M. Knite, S. Oras, T. Käämbre, S. Vlassov, M. Antsov, M. Timusk and A. Šutka, *Macromol. Mater. Eng.*, 2019, **305**, 1900638.
- 99 J. H. Lee, K. H. Kim, M. Choi, J. Jeon, H. J. Yoon, J. Choi, Y. S. Lee, M. Lee and J. J. Wie, *Nano Energy*, 2019, **66**, 104158.
- 100 W. He, C. Shan, H. Wu, S. Fu, Q. Li, G. Li, X. Zhang, Y. Du, J. Wang, X. Wang and C. Hu, *Adv. Energy Mater.*, 2022, **12**, 2201454.
- 101 H. Wu, S. Fu, W. He, C. Shan, J. Wang, Y. Du, S. Du, B. Li and C. Hu, *Adv. Funct. Mater.*, 2022, **32**, 2203884.
- 102 Y. H. Yu and X. D. Wang, *Extreme Mech. Lett.*, 2016, **9**, 514–530.
- 103 Y. H. Liu, J. L. Mo, Q. Fu, Y. X. Lu, N. Zhang, S. F. Wang and S. X. Nie, *Adv. Funct. Mater.*, 2020, **30**, 202004714.
- 104 A. Šutka, K. Malnieks, L. Lapčinskis, M. Timusk, K. Pudzs and M. Rutkis, *iScience*, 2020, **23**, 101011.
- 105 X. Tao, J. Nie, S. Li, Y. Shi, S. Lin, X. Chen and Z. L. Wang, *ACS Nano*, 2021, **15**, 10609–10617.
- 106 S. Lin, X. Chen and Z. L. Wang, *Chem. Rev.*, 2022, **122**, 5209–5232.
- 107 Z. Cui, E. Drioli and Y. M. Lee, *Prog. Polym. Sci.*, 2014, **39**, 164–198.
- 108 X. Wang, Y. Shi, P. Yang, X. Tao, S. Li, R. Lei, Z. Liu, Z. L. Wang and X. Chen, *Small*, 2022, **18**, 2107232.
- 109 J. Choi, S. Won, H. J. Yoon, J. H. Lee, H. W. Jang, J. Jeon, A. Y. Kim, S. H. Park, J. H. Youk, M. Lee and J. J. Wie, *Nano Energy*, 2022, **92**, 106761.
- 110 H. Oh, E. Jo, H. W. Jang, H. Jung, S. H. Park, A. Y. Kim, J. H. Jung, J. H. Youk and M. Lee, *Extreme Mech. Lett.*, 2022, **50**, 101533.
- 111 H. Jaewook, C. Jihoon, K. SeongMin, K. Jong Hun, S. Seungmin, P. Jeong Young, L. Sangmin and K. Jin-Baek, *Nano Energy*, 2017, **36**, 126–133.
- 112 R. Krishnan and A. Parthiban, *Eur. Polym. J.*, 2018, **101**, 66–76.
- 113 K. Ranganathan and A. Parthiban, *Polymer*, 2018, **135**, 295–304.
- 114 J. W. Lee, S. Jung, T. W. Lee, J. Jo, H. Y. Chae, K. Choi, J. J. Kim, J. H. Lee, C. Yang and J. M. Baik, *Adv. Energy Mater.*, 2019, **9**, 1901987.
- 115 X. Tao, S. Li, Y. Shi, X. Wang, J. Tian, Z. Liu, P. Yang, X. Chen and Z. L. Wang, *Adv. Funct. Mater.*, 2021, **31**, 2106082.
- 116 J. Wu, X. L. Wang, J. Y. He, Z. H. Li and L. Z. Li, *J. Mater. Chem. A*, 2021, **9**, 6583–6590.
- 117 S. S. Kwak, S. M. Kim, H. Ryu, J. Kim, U. Khan, H. J. Yoon, Y. H. Jeong and S. W. Kim, *Energy Environ. Sci.*, 2019, **12**, 3156–3163.
- 118 H. M. Chen, Z. Z. Sun, H. H. Lin, C. B. He and D. S. Mao, *Adv. Funct. Mater.*, 2022, **32**, 2204263.
- 119 J. Kim, D. Kang, H. K. Lee, J. H. Hwang, H. Y. Lee, S. Jeon, D. Kim, S. Kim and S. W. Kim, *Adv. Funct. Mater.*, 2023, **33**, 2209648.
- 120 W. Intarabumrung, S. Kuntharin, V. Harnchana, T. Prada, P. Kasemsiri, A. J. Hunt and N. Supanchaiyamat, *ACS Sustain.*, 2022, **10**, 13680–13691.
- 121 P. K. Sarkar, T. Kamilya and S. Acharya, *ACS Appl. Energy Mater.*, 2019, **2**, 5507–5514.
- 122 C. Y. Zhang, J. L. Mo, Q. Fu, Y. H. Liu, S. F. Wang and S. X. Nie, *Nano Energy*, 2021, **81**, 105637.
- 123 P. Ding, J. Chen, U. Farooq, P. Zhao, N. Soin, L. Yu, H. Jin, X. Wang, S. Dong and J. Luo, *Nano Energy*, 2018, **46**, 63–72.
- 124 H. G. Menge, N. D. Huynh, H. J. Hwang, S. Han, D. Choi and Y. T. Park, *ACS Energy Lett.*, 2021, **6**, 2451–2459.
- 125 T. A. L. Burgo, B. C. Batista and F. Galembeck, *ACS Omega*, 2017, **2**, 8940–8947.
- 126 Z. Liu, S. Li, S. Lin, Y. Shi, P. Yang, X. Chen and Z. L. Wang, *Nano Lett.*, 2022, **22**, 4074–4082.
- 127 A. Šutka, L. Lapčinskis, O. Verners, L. Ģērmane, K. Smits, A. Pludons, S. Gaidukovs, I. Jerāne, M. Zubkins, K. Pudzs, P. C. Sherrell and J. Blums, *Adv. Mater. Technol.*, 2022, **7**, 2200162.
- 128 S. Y. Ding and W. Wang, *Chem. Soc. Rev.*, 2013, **42**, 548–568.
- 129 Z. Wang, S. Zhang, Y. Chen, Z. Zhang and S. Ma, *Chem. Soc. Rev.*, 2020, **49**, 708–735.
- 130 J. Li, X. Jing, Q. Li, S. Li, X. Gao, X. Feng and B. Wang, *Chem. Soc. Rev.*, 2020, **49**, 3565–3604.
- 131 X. Zhao, P. Pachfule and A. Thomas, *Chem. Soc. Rev.*, 2021, **50**, 6871–6913.
- 132 S. Yuan, X. Li, J. Zhu, G. Zhang, P. Van Puyvelde and B. Van der Bruggen, *Chem. Soc. Rev.*, 2019, **48**, 2665–2681.
- 133 J. Y. Zhu, S. S. Yuan, J. Wang, Y. T. Zhang, M. M. Tian and B. Van der Bruggen, *Prog. Polym. Sci.*, 2020, **110**, 101308.
- 134 C. Y. Lin, D. Zhang, Z. Zhao and Z. Xia, *Adv. Mater.*, 2018, **30**, 1703646.
- 135 K. Y. Geng, V. Arumugam, H. J. Xu, Y. N. Gao and D. L. Jiang, *Prog. Polym. Sci.*, 2020, **108**, 101288.
- 136 L. P. Zhai, W. T. Wei, B. W. Ma, W. Y. Ye, J. Wang, W. H. Chen, X. B. Yang, S. W. Cui, Z. J. Wu, C. Soutis, G. S. Zhu and L. W. Mi, *ACS Mater. Lett.*, 2020, **2**, 1691–1697.
- 137 C. Lin, L. Sun, X. Meng, X. Yuan, C. X. Cui, H. Qiao, P. Chen, S. Cui, L. Zhai and L. Mi, *Angew. Chem., Int. Ed.*, 2022, **61**, 202211601.
- 138 L. Zhai, S. Cui, B. Tong, W. Chen, Z. Wu, C. Soutis, D. Jiang, G. Zhu and L. Mi, *Chemistry*, 2020, **26**, 5784–5788.
- 139 S. Hajra, J. Panda, J. Swain, H. G. Kim, M. Sahu, M. K. Rana, R. Samantaray, H. J. Kim and R. Sahu, *Nano Energy*, 2022, **101**, 107620.
- 140 L. Shi, V. S. Kale, Z. N. Tian, X. M. Xu, Y. J. Lei, S. Kandambeth, Y. Z. Wang, P. T. Parvatkar, O. Shekhah, M. Eddaoudi and H. N. Alshareef, *Adv. Funct. Mater.*, 2023, **33**, 2212891.
- 141 X. Zhang, X. Huang, S. W. Kwok and S. Soh, *Adv. Mater.*, 2016, **28**, 3024–3029.
- 142 Y. Shang, Z. Wang, C. Yu, W. Xu, Z. Chen, B. Jiang and H. Zhang, *Nano Energy*, 2022, **103**, 107847.
- 143 J. Wu, X. L. Wang, H. Q. Li, F. Wang and Y. Q. Hu, *Nano Energy*, 2019, **63**, 103864.
- 144 P. Martins, A. C. Lopes and S. Lanceros-Mendez, *Prog. Polym. Sci.*, 2014, **39**, 683–706.

- 145 J. W. Lee, H. J. Cho, J. Chun, K. N. Kim, S. Kim, C. W. Ahn, I. W. Kim, J. Y. Kim, S. W. Kim, C. Yang and J. M. Baik, *Sci. Adv.*, 2017, **3**, e1602902.
- 146 X. Tao, S. Fu, S. Li, Z. Liu, P. Yang, C. Liu, S. Lin, S. Zhang, X. Chen, X. Jian and Z. L. Wang, *Small Methods*, 2023, **7**, 2201593.
- 147 J. Kim, J. H. Lee, H. Ryu, J. H. Lee, U. Khan, H. Kim, S. S. Kwak and S. W. Kim, *Adv. Funct. Mater.*, 2017, **27**, 1700702.
- 148 K. Y. Lee, S. K. Kim, J. H. Lee, D. Seol, M. K. Gupta, Y. Kim and S. W. Kim, *Adv. Funct. Mater.*, 2016, **26**, 3067–3073.
- 149 P. Bai, G. Zhu, Y. S. Zhou, S. H. Wang, J. S. Ma, G. Zhang and Z. L. Wang, *Nano Res.*, 2014, **7**, 990–997.
- 150 A. Šutka, K. Mālnieks, A. Linarts, M. Timusk, V. Jurkāns, I. Gorņevs, J. Blūms, A. Bērziņa, U. Joost and M. Knite, *Energy Environ. Sci.*, 2018, **11**, 1437–1443.
- 151 R. M. Michell and A. J. Muller, *Prog. Polym. Sci.*, 2016, **54–55**, 183–213.
- 152 Y. S. Choi, Q. S. Jing, A. Datta, C. Boughey and S. Kar-Narayan, *Energy Environ. Sci.*, 2017, **10**, 2180–2189.
- 153 Y. S. Choi, S. K. Kim, M. Smith, F. Williams, M. E. Vickers, J. A. Elliott and S. Kar-Narayan, *Sci. Adv.*, 2020, **6**, eaay5065.
- 154 Z. Liu, Y. z Huang, Y. Shi, X. Tao, P. Yang, X. Dong, J. Hu, Z. X. Huang, X. Chen and J. P. Qu, *Adv. Funct. Mater.*, 2023, 2302164.
- 155 J. J. Wei and L. Zhu, *Prog. Polym. Sci.*, 2020, **106**, 101254.
- 156 X. Y. Huang, B. Sun, Y. K. Zhu, S. T. Li and P. K. Jiang, *Prog. Mater. Sci.*, 2019, **100**, 187–225.
- 157 X. Du, Y. Liu, J. Wang, H. Niu, Z. Yuan, S. Zhao, X. Zhang, R. Cao, Y. Yin, N. Li, C. Zhang, Y. Xing, W. Xu and C. Li, *ACS Appl. Mater. Interfaces*, 2018, **10**, 25683–25688.
- 158 L. Lapčinskis, K. Mālnieks, A. Linarts, J. Blūms, K. N. Šmits, M. Järvekūlg, M. R. Knite and A. Šutka, *ACS Appl. Energy Mater.*, 2019, **2**, 4027–4032.
- 159 J. Wang, H. Y. Wu, Z. Wang, W. C. He, C. C. Shan, S. K. Fu, Y. Du, H. Liu and C. G. Hu, *Adv. Funct. Mater.*, 2022, **32**, 2204322.
- 160 H. Wu, W. He, C. Shan, Z. Wang, S. Fu, Q. Tang, H. Guo, Y. Du, W. Liu and C. Hu, *Adv. Mater.*, 2022, **34**, 2109918.
- 161 D. K. Bharti, S. Veeralingam and S. Badhulika, *Mater. Horiz.*, 2022, **9**, 663–674.
- 162 J. Chen, H. Guo, X. He, G. Liu, Y. Xi, H. Shi and C. Hu, *ACS Appl. Mater. Interfaces*, 2016, **8**, 736–744.
- 163 W. Seung, H. J. Yoon, T. Y. Kim, H. Ryu, J. Kim, J. H. Lee, J. H. Lee, S. Kim, Y. K. Park, Y. J. Park and S. W. Kim, *Adv. Energy Mater.*, 2017, **7**, 1600988.
- 164 Y. Park, Y. E. Shin, J. Park, Y. Lee, M. P. Kim, Y. R. Kim, S. Na, S. K. Ghosh and H. Ko, *ACS Nano*, 2020, **14**, 7101–7110.
- 165 H. W. Park, N. D. Huynh, W. Kim, C. Lee, Y. Nam, S. Lee, K. B. Chung and D. Choi, *Nano Energy*, 2018, **50**, 9–15.
- 166 C. Wu, T. W. Kim, J. H. Park, H. An, J. Shao, X. Chen and Z. L. Wang, *ACS Nano*, 2017, **11**, 8356–8363.
- 167 N. Cui, L. Gu, Y. Lei, J. Liu, Y. Qin, X. Ma, Y. Hao and Z. L. Wang, *ACS Nano*, 2016, **10**, 6131–6138.
- 168 P. Manchi, S. A. Graham, H. Patnam, M. V. Paranjape and J. S. Yu, *Small*, 2022, **18**, 2200822.
- 169 J. Kim, H. Ryu, J. H. Lee, U. Khan, S. S. Kwak, H. J. Yoon and S. W. Kim, *Adv. Energy Mater.*, 2020, **10**, 1903524.
- 170 M. M. Hasan, M. S. B. Sadeque, I. Albasar, H. Pecenek, F. K. Dokan, M. S. Onses and M. Ordu, *Small*, 2023, **19**, 2206107.
- 171 P. Sahatiya, S. Kannan and S. Badhulika, *Appl. Mater. Today*, 2018, **13**, 91–99.
- 172 M. Sahu, V. Vivekananthan, S. Hajra, K. S. Abisegapriyan, N. P. M. J. Raj and S. J. Kim, *J. Mater. Chem. A*, 2020, **8**, 22257–22268.
- 173 J. Du, X. Y. Yang, J. L. Duan, Y. D. Wang and Q. W. Tang, *Nano Energy*, 2020, **70**, 104514.
- 174 G. Q. Gu, C. B. Han, J. J. Tian, C. X. Lu, C. He, T. Jiang, Z. Li and Z. L. Wang, *ACS Appl. Mater. Interfaces*, 2017, **9**, 11882–11888.
- 175 J. S. Im and I. K. Park, *ACS Appl. Mater. Interfaces*, 2018, **10**, 25660–25665.
- 176 D. L. Vu and K. K. Ahn, *Polymers*, 2022, **14**, 1547.
- 177 Y. Yu, Z. Li, Y. Wang, S. Gong and X. Wang, *Adv. Mater.*, 2015, **27**, 4938–4944.
- 178 J. W. Lee, S. Jung, J. Jo, G. H. Han, D.-M. Lee, J. Oh, H. J. Hwang, D. Choi, S.-W. Kim, J. H. Lee, C. Yang and J. M. Baik, *Energy Environ. Sci.*, 2021, **14**, 1004–1015.
- 179 S. Cha, Y. Cho, J. G. Kim, H. Choi, D. Ahn, J. Sun, D. S. Kang, C. Pak and J. J. Park, *Small Methods*, 2022, **6**, 2101545.
- 180 L. Jin, X. Xiao, W. Deng, A. Nashalian, D. He, V. Raveendran, C. Yan, H. Su, X. Chu, T. Yang, W. Li, W. Yang and J. Chen, *Nano Lett.*, 2020, **20**, 6404–6411.
- 181 J. X. Zhong, X. J. Hou, J. He, F. Xue, Y. Yang, L. Chen, J. B. Yu, J. L. Mu, W. P. Geng and X. J. Chou, *Nano Energy*, 2022, **98**, 107289.
- 182 M. Vafaiee, F. Ejehi and R. Mohammadpour, *Sci. Rep. Hokkaido Fish. Exp. Stn*, 2023, **13**, 370.
- 183 H. Wang, M. Shi, K. Zhu, Z. Su, X. Cheng, Y. Song, X. Chen, Z. Liao, M. Zhang and H. Zhang, *Nanoscale*, 2016, **8**, 18489–18494.
- 184 N. Kaur, J. Bahadur, V. Panwar, P. Singh, K. Rath and K. Pal, *Sci. Rep.*, 2016, **6**, 38835.
- 185 T. Huang, M. Lu, H. Yu, Q. Zhang, H. Wang and M. Zhu, *Sci. Rep.*, 2015, **5**, 13942.
- 186 P. L. Liu, N. Sun, Y. Y. Mi, X. H. Luo, X. X. Dong, J. Y. Cai, X. L. Jia, M. A. Ramos, T. S. Hu and Q. Xu, *Compos. Sci. Technol.*, 2021, **208**, 108733.
- 187 Z. Liu, K. Wang, X. Jiang, M. S. Javed and W. Han, *Appl. Phys. Lett.*, 2022, **121**, 113902.
- 188 V. Harnchana, H. V. Ngoc, W. He, A. Rasheed, H. Park, V. Amornkitbamrung and D. J. Kang, *ACS Appl. Mater. Interfaces*, 2018, **10**, 25263–25272.
- 189 S. Parandeh, M. Kharaziha and F. Karimzadeh, *Nano Energy*, 2019, **59**, 412–421.
- 190 Y. H. Wu, Y. Luo, J. K. Qu, W. A. Daoud and T. Qi, *Nano Energy*, 2019, **64**, 103948.
- 191 H. Ryu, J. H. Lee, T. Y. Kim, U. Khan, J. H. Lee, S. S. Kwak, H. J. Yoon and S. W. Kim, *Adv. Energy Mater.*, 2017, **7**, 1700289.



- 192 H. J. Hwang, J. S. Kim, W. Kim, H. Park, D. Bhatia, E. Jee, Y. S. Chung, D. Kim and D. Choi, *Adv. Energy Mater.*, 2019, **9**, 1803786.
- 193 Y. C. Lai, H. M. Wu, H. C. Lin, C. L. Chang, H. H. Chou, Y. C. Hsiao and Y. C. Wu, *Adv. Funct. Mater.*, 2019, **29**, 1904626.
- 194 L. Jia, Z. H. Guo, L. Li, C. Pan, P. Zhang, F. Xu, X. Pu and Z. L. Wang, *ACS Nano*, 2021, **15**, 19651–19660.
- 195 W. Xu, L.-B. Huang, M.-C. Wong, L. Chen, G. Bai and J. Hao, *Adv. Energy Mater.*, 2017, **7**, 1601529.
- 196 X. X. Luo, L. P. Zhu, Y. C. Wang, J. Y. Li, J. J. Nie and Z. L. Wang, *Adv. Funct. Mater.*, 2021, **31**, 202104928.
- 197 Y. Wu, Y. Luo, T. J. Cuthbert, A. V. Shokurov, P. K. Chu, S. P. Feng and C. Menon, *Adv. Sci.*, 2022, **9**, 2106008.
- 198 Z. Jin, F. Zhao, Y. Lei and Y.-C. Wang, *Nano Energy*, 2022, **95**, 106988.
- 199 M. Zhang, R. Yu, X. Tao, Y. He, X. Li, F. Tian, X. Chen and W. Huang, *Adv. Funct. Mater.*, 2023, **33**, 2208083.
- 200 M. Zhang, X. Tao, R. Yu, Y. He, X. Li, X. Chen and W. Huang, *J. Mater. Chem. A*, 2022, **10**, 12005–12015.
- 201 G. Suo, Y. Yu, Z. Zhang, S. Wang, P. Zhao, J. Li and X. Wang, *ACS Appl. Mater. Interfaces*, 2016, **8**, 34335–34341.
- 202 Y. Yang, H. L. Zhang, J. Chen, S. M. Lee, T. C. Hou and Z. L. Wang, *Energy Environ. Sci.*, 2013, **6**, 1744–1749.
- 203 D. Park, S. H. Shin, I. J. Yoon and J. Nah, *Nanotechnology*, 2018, **29**, 185402.
- 204 X. He, H. Guo, X. Yue, J. Gao, Y. Xi and C. Hu, *Nanoscale*, 2015, **7**, 1896–1903.
- 205 R. M. Wen, J. M. Guo, A. F. Yu, J. Y. Zhai and Z. L. Wang, *Adv. Funct. Mater.*, 2019, **29**, 1807655.
- 206 C. Ye, D. Liu, P. Chen, L. N. Y. Cao, X. Li, T. Jiang and Z. L. Wang, *Adv. Mater.*, 2023, **35**, 2209713.
- 207 X. T. Xu, P. Y. Li, Y. T. Ding, W. H. Xu, S. Y. Liu, Z. M. Zhang, Z. K. Wang and Z. B. Yang, *Energy Environ. Sci.*, 2022, **15**, 2916–2926.
- 208 L. Xie, L. Yin, Y. Liu, H. Liu, B. Lu, C. Zhao, T. A. Khattab, Z. Wen and X. Sun, *ACS Nano*, 2022, **16**, 5292–5302.
- 209 R. Cheng, K. Dong, L. Liu, C. Ning, P. Chen, X. Peng, D. Liu and Z. L. Wang, *ACS Nano*, 2020, **14**, 15853–15863.
- 210 Q. Guan, X. Lu, Y. Chen, H. Zhang, Y. Zheng, R. E. Neisiany and Z. You, *Adv. Mater.*, 2022, **34**, 2204543.
- 211 D. Zhang, W. Yang, W. Gong, W. Ma, C. Hou, Y. Li, Q. Zhang and H. Wang, *Adv. Mater.*, 2021, **33**, 2100782.
- 212 W. Gong, C. Hou, J. Zhou, Y. Guo, W. Zhang, Y. Li, Q. Zhang and H. Wang, *Nat. Commun.*, 2019, **10**, 868.
- 213 W. Yang, W. Gong, C. Hou, Y. Su, Y. Guo, W. Zhang, Y. Li, Q. Zhang and H. Wang, *Nat. Commun.*, 2019, **10**, 5541.
- 214 Q. Zheng, Y. Zou, Y. Zhang, Z. Liu, B. Shi, X. Wang, Y. Jin, H. Ouyang, Z. Li and Z. L. Wang, *Sci. Adv.*, 2016, **2**, e1501478.
- 215 R. Wang, L. Mu, Y. Bao, H. Lin, T. Ji, Y. Shi, J. Zhu and W. Wu, *Adv. Mater.*, 2020, **32**, 2002878.
- 216 W. Jiang, H. Li, Z. Liu, Z. Li, J. Tian, B. Shi, Y. Zou, H. Ouyang, C. Zhao, L. Zhao, R. Sun, H. Zheng, Y. Fan, Z. L. Wang and Z. Li, *Adv. Mater.*, 2018, **30**, 1801895.
- 217 J. H. Lee, R. Hinchet, S. K. Kim, S. Kim and S. W. Kim, *Energy Environ. Sci.*, 2015, **8**, 3605–3613.
- 218 G. I. Dzhardimalieva, B. C. Yadav, S. E. Kudaibergenov and I. E. Uflyand, *Polymers*, 2020, **12**, 2594.
- 219 P. P. Zhang, Y. H. Chen, Z. H. Guo, W. B. Guo, X. Pu and Z. L. Wang, *Adv. Funct. Mater.*, 2020, **30**, 201909252.
- 220 F. Jiang, X. Zhou, J. Lv, J. Chen, J. Chen, H. Kongcharoen, Y. Zhang and P. S. Lee, *Adv. Mater.*, 2022, **34**, 2200042.
- 221 K. Parida, V. Kumar, W. Jiangxin, V. Bhavanasi, R. Bendi and P. S. Lee, *Adv. Mater.*, 2017, **29**, 1702181.
- 222 Z. Ren, Y. Ding, J. Nie, F. Wang, L. Xu, S. Lin, X. Chen and Z. L. Wang, *ACS Appl. Mater. Interfaces*, 2019, **11**, 6143–6153.
- 223 S. Jang, M. La, S. Cho, Y. Yun, J. H. Choi, Y. Ra, S. J. Park and D. Choi, *Nano Energy*, 2020, **70**, 104541.
- 224 T. Krupenkin and J. A. Taylor, *Nat. Commun.*, 2011, **2**, 448.
- 225 H. Yang, S. Hong, B. Koo, D. Lee and Y. B. Kim, *Nano Energy*, 2017, **31**, 450–455.
- 226 M. Amin Diab, *Eur. Polym. J.*, 1984, **20**, 599–603.
- 227 A. E. Tonelli, G. Khanarian and R. E. Cais, *Macromolecules*, 2002, **18**, 2324–2326.
- 228 O. Vogl, M. F. Qin and A. Zilkha, *Prog. Polym. Sci.*, 1999, **24**, 1481–1525.
- 229 J. Q. Xiong, M. F. Lin, J. X. Wang, S. L. Gaw, K. Parida and P. S. Lee, *Adv. Energy Mater.*, 2017, **7**, 201701243.
- 230 B. Zhang, C. Zhang, O. Yang, W. Yuan, Y. Liu, L. He, Y. Hu, Z. Zhao, L. Zhou, J. Wang and Z. L. Wang, *ACS Nano*, 2022, **16**, 15286–15296.
- 231 Q. K. Ye, Y. Z. Wu, Y. Y. Qi, L. Shi, S. Y. Huang, L. Zhang, M. L. Li, W. Li, X. Y. Zeng, H. L. Wo, X. Z. Wang, S. R. Dong, S. Ramakrishna and J. K. Luo, *Nano Energy*, 2019, **61**, 381–388.
- 232 S. Chatterjee, G. H. Major, B. M. Lunt, M. Kaykhaii and M. R. Linfoord, *Microsc. Microanal.*, 2016, **22**, 964–970.
- 233 S. Lin, X. Li, K. Wang, T. Shang, L. Zhou, L. Zhang, J. Wang and N. Huang, *Polymers*, 2019, **11**, 734.